FRONT MATTER

Title

- Full Title: Newly repopulated spinal cord microglia exhibit a unique transcriptome and coincide with sex-independent pain resolution
- Short Title: Repopulated microglia and pain resolution

Authors

Lauren J. Donovan[1†], Caldwell M. Bridges[1†], Amy R. Nippert[1], Meng Wang[2], Shaogen Wu[1], Thomas E. Forman[1], Elena S. Haight[1], Nolan A. Huck[1], Claire E. Jordan[1], Aysha S. Gardner[1], Ramesh V. Nair[2], Vivianne L. Tawfik[1*]

Afilliations

[1] Department of Anesthesiology, Perioperative and Pain Medicine, Stanford University, Stanford, CA 94305, USA
[2] Stanford Center for Genomics and Personalized Medicine, Stanford University School of Medicine, Stanford, CA 94304, USA

[†] These authors contributed equally

[*] Correspondence should be addressed to
Vivianne L. Tawfik, MD, PhD
Department of Anesthesiology, Perioperative & Pain Medicine
300 Pasteur Drive, E.D. Stone Grant Building, S007
Stanford, CA 94305
Ph: 1-650-724-7935
Email: vivianne@stanford.edu
Twitter: @TawfikLab
ORCID ID: 0000-0002-4422-2014

Abstract

Microglia contribute to the initiation of pain, however, a translationally viable approach addressing how or when to modulate these cells remains elusive. We used a targeted, inducible genetic microglial depletion strategy at both the acute and acute-to-chronic transition phases in the clinically-relevant tibial fracture/casting model to determine the contribution of microglia to the initiation and maintenance of pain. We observed complete resolution of pain after transient microglial depletion at the acute-to-chronic phase, which coincided with the timeframe of full repopulation of microglia. These repopulated microglia were morphologically distinct from control microglia, suggesting they may exhibit a unique transcriptome. RNA sequencing of repopulated spinal cord microglia identified genes of interest using weighted gene co-expression network analysis (WGCNA). We intersected these genes with a newly-generated single nuclei microglial dataset from human dorsal horn spinal cord to identify human-relevant genes that may promote homeostatic features of microglia and ultimately promote pain resolution after injury.

Teaser

Microglial depletion/repopulation resolves pain after peripheral injury and repopulated microglia exhibit a unique transcriptome

MAIN TEXT

Introduction

The transition to chronic pain is still poorly understood even though persistent pain affects one in three individuals.(1) Injury-induced neuronal hyperactivation leads to downstream engagement of microglia in the spinal cord,(2) that contributes to the initiation of pain.(3, 4) This has been confirmed in several preclinical pain models in which direct inhibition of spinal microglia with a Gi DREADD,(5) reversal of microglial activation(6-8) or inhibition of spinal microgliosis(9) decreases nociceptive outcomes such as allodynia and thermal hyperalgesia. Additionally, depletion of microglia using either the immunotoxin Mac1-saporin,(10, 11) or transgenic Cx3CR1-Cre$^{ERT2\text{-}eYFP}$;R26-iDTR^{LSL} mice(12) prevents or reverses existing pain when tested at limited time points after nerve injury. Importantly, after genetic depletion, microglia fully repopulate the CNS within 14 days.(12, 13) Therefore it is possible that either reactive microglia initiate the transition from acute-to-chronic pain, or repopulated microglia actively resolve pain. The reversal of pain after transient depletion of microglia offers an opportunity to study the contribution of microglia in a pain-resolution context.

While microglial “signatures genes" have been identified, transcriptomic studies highlight that microglia are heterogeneous cells which are phenotypically and genetically shaped by their microenvironment,(14, 15) particularly by their exact anatomic location.(16) Importantly, the majority of these studies have been performed in distinct brain supraspinal regions(17, 18) with few to date undertaking transcriptomic analysis of microglia from the mouse spinal cord(19, 20) and even fewer performing such analyses in human spinal cord tissue.(21) Additionally, transcriptomic analyses of CNS tissue in disease states involving neuroinflammation, such as Alzheimer’s,(22) multiple sclerosis,(23) and chronic pain,(20) suggest heterogeneity in microglial responses to pathology. In-depth knowledge of the specific transcriptome of spinal cord microglia after pain-producing peripheral injury is therefore needed to identify markers for further targeted drug development for the treatment of chronic pain. Additionally, because these data are often collected in rodent models, the use of single-cell sequencing data from human spinal cord is necessary to improve development of clinically translatable microglia-directed pain therapeutics.

In this study, we evaluated the temporal contribution of microglia to pain progression using targeted genetic microglia depletion with Cx3CR1-Cre$^{ERT2\text{-}eYFP}$;R26-iDTR^{LSL} mice in the context of peripheral injury. We used the clinically-relevant tibial fracture/casting model of complex regional pain syndrome (CRPS) which, in contrast to other injury models, has a distinctly timed acute-to-chronic pain transition. We discovered that microglial depletion/repopulation at the acute-to-chronic transition completely resolved pain and improved peripheral inflammation. We took advantage of this pain resolution context to establish transcriptomic signatures of repopulated spinal cord microglia at the point of full repopulation, which coincides with behavioral improvements in pain. Finally, we identified targets with human relevance by intersecting mouse genes of interest identified by weighted gene co-expression network analysis (WGCNA) with a newly generated human spinal cord single nuclei microglial transcriptome dataset.

Results

Morphologically distinct microglia repopulate the spinal cord 14 days after targeted genetic depletion

We utilized a mouse line (Cx3CR1-Cre$^{ERT2\text{-}eYFP}$; R26-iDTR^{LSL}) which allows for temporally controlled depletion of microglia, without depletion of other myeloid-lineage cells (ex. peripheral macrophages, Figure 1a). Tamoxifen is administered to express the diphtheria toxin receptor (DTR) in CX3CR1+ cells, then diphtheria toxin (DT) is administered 3-4 weeks later, giving time for peripheral macrophages to turn over, and no longer express the DTR. While these mice have been previously characterized,(13) we independently confirmed that the Cx3CR1- Cre$^{ERT2\text{-}eYFP}$ mouse was tamoxifen dependent in a parallel study.(8) After DT-induced depletion, microglia repopulate to baseline numbers over the course of ~14 days (Figure 1b-d), consistent with previous studies.(12, 13, 24) Interestingly, these repopulated microglia remained morphologically distinct when compared to baseline control microglia, with fewer, shorter branches and an overall diminished complexity even at 14 days post-depletion/repopulation (Figure 1e-f).

We have previously demonstrated that the tibial fracture/casting model of CRPS results in signs of peripheral inflammation (paw edema, increased paw temperature) lasting up to 4 weeks post-injury. In contrast, mechanical paw sensitivity (allodynia) persists for at least 20 weeks.(8, 25) These findings suggest a peripheral-to-central (or acute-to-chronic) transition between 3- and 5-weeks post-injury. Importantly, microglia depletion alone did not affect baseline weight bearing, paw edema or paw temperature (Supplemental Figure 1). Additionally, microglial depletion alone had no effect on measures of nociception, including unchanged mechanical sensitivity (Figure 1g) and hot plate latency (Figure 1h).

Microglial depletion at the acute-to-chronic transition drastically improves pain trajectory

To establish the contribution of microglia to persistent pain, we first performed microglial depletion at the time of injury (day 0, acute phase) in the tibial fracture/casting model of CRPS (Supplemental Figure 2a). When microglia were depleted in this preventative paradigm, both male and female injured mice with microglial depletion (Injured-Depleted) demonstrated a significant but partial attenuation of allodynia over the course of the 9-week testing period, compared with sex-matched injured-only controls (Supplemental Figure 2b). The latency to withdrawal on a hot plate was significantly increased in females ($p = 0.0304$) but not males ($p = 0.0780$), in the Injured-Depleted groups (Supplemental Figure 2c-d). Both male and female Injured-Depleted mice improved their weight bearing on the injured hind paw at 4 weeks after injury (Supplemental Figure 2e-f), exhibited less edema (Supplemental Figure 2g-h), and less warmth (Supplemental Figure 2i-j) of the injured limb.

Due to the incomplete reversal of allodynia in the preventive acute phase depletion paradigm, as well as the clinical relevance of post-injury treatment, we next tested microglia depletion at 3 weeks post-fracture (acute-to-chronic phase, Figure 2a). Strikingly, we found that both male and female Injured-Depleted mice demonstrated a profound improvement in allodynia with a return to pre-injury baseline values over the course of the testing period (Figure 2b). The reversal of mechanical hypersensitivity was particularly remarkable as the mice were allodynic immediately after DT treatment (when

microglia were absent/depleted); then exhibited a progressively improving pain trajectory that temporally paralleled full spinal cord repopulation of microglia. We additionally observed an increase in hot plate latency in both male and female Injured-Depleted mice as well as improvement in weight bearing, edema, and warmth of the injured paw at 4 weeks in the Injured-Depleted mice (Figure 2c-d). These findings suggest that microglial repopulation, and not depletion itself, may trigger pain resolution and improvement in classic peripheral signs of CRPS (edema and temperature) in a post-injury/treatment paradigm.

Sequencing of repopulated microglia reveals a distinct transcriptome that may contribute to pain resolution

In our model, morphologically distinct microglia repopulated by 14 days post-depletion, coincident with a sustained improvement in pain and peripheral inflammatory outcomes. To identify transcripts that may enable repopulated microglia to have a pro-resolution role in the context of peripheral injury, we FACS-isolated microglia from the lumbar spinal cord at 5 weeks post-injury (14 days post-microglia depletion/repopulation) for subsequent RNA sequencing from 4 groups: uninjured mice with resident microglia (Uninjured-Resident microglia), uninjured mice with repopulated microglia (Uninjured-Repopulated microglia), injured mice with resident microglia (Injured-Resident microglia) and injured mice with repopulated microglia (Injured-Repopulated microglia).

We sorted microglia as follows: live (SYTOX blue negative), $CD19^{-}CD3^{-}CD45^{mid}CD11b^{+}Cx3CR1\text{-}YFP^{+}$ (Supplemental Figure 3a). To first confirm the specificity of our isolation method for CNS microglia, we used the publicly available ImmGen "My GeneSet" program to cross-reference genes in our male RNAseq dataset with the ImmGen database of over 50 cell populations.(26) The top 100 genes expressed by log2(cpm+1) in our datasets clearly defined a microglia-specific signature that could be differentiated from similar myeloid-lineage cells including blood monocytes (Supplemental Figure 3b). We next performed multidimensional scaling (MDS) and observed stronger clustering of microglial gene profiles by treatment group in males compared to females, with microglia depletion having the greatest effect (Supplemental Figure 4).

Differential gene expression analysis using DESeq2 was performed on the microglial transcriptome for four comparisons by sex (Supplemental Figure 5): Injured-Resident microglia vs. Uninjured-Resident microglia (effect of injury alone), Uninjured-Repopulated microglia vs. Uninjured-Resident microglia (effect of microglia depletion/repopulation), Injured-Repopulated microglia vs. Uninjured-Repopulated microglia (effect of injury in the context of microglia depletion/repopulation), Injured-Repopulated microglia vs. Injured-Resident microglia (effect of microglia depletion/repopulation in the context of injury). The analyses were performed at the transcript level for increased resolution and then transcripts were mapped to their corresponding genes for data representation, as indicated. For females we identified 26,748 transcripts which mapped to 12,020 unique genes. For males we identified 28,345 transcripts which mapped to 11,999 unique genes. Consistent with datasets from other pain models(27), the number of differentially expressed genes (DEGs) in sorted microglia in the injury alone context (Injured-Resident microglia vs Uninjured-Resident microglia) was limited. For females there were no upregulated DEGs and just one downregulated

DEG (*H2-Q7*), while for males there were 30 upregulated DEGs and 2 downregulated DEGs, none of which overlapped between sexes (Supplemental Table S1 and Extended Data 1). Also consistent with prior datasets,(13) microglial depletion/repopulation resulted in many DEGs (Uninjured-Repopulated microglia vs Uninjured-Resident microglia), especially in males, indicating that repopulated microglia are distinctly different from microglia at baseline. Specifically, for males there were 571 upregulated DEGs and 494 downregulated DEGs, while for females there were 15 upregulated DEGs and 63 downregulated DEGs (Supplemental Table S1). The effect of injury in the context of microglia depletion (Injured-Repopulated microglia vs Uninjured-Repopulated microglia) had fewer overall DEGs and was also sex-specific. For males there were 92 upregulated DEGs and 7 downregulated DEGs, while for females there were 19 upregulated DEGs and 34 downregulated DEGs, none of which overlapped between sexes (Supplemental Table S1). These gene changes indicate that repopulated microglia in the context of injury are distinct from repopulated microglia without injury.

To characterize microglia that repopulate in the context of peripheral injury but no longer contribute to sensitization (pain resolution context), we focused our subsequent analyses on the Injured-Repopulated microglia versus Injured-Resident microglia comparison. We identified numerous DEGs with several shared by both sexes. For males there were 412 upregulated DEGs and 283 downregulated DEGs, while for females there were 94 upregulated DEGs and 173 downregulated DEGs (Figure 3a and Extended Data 1). In total, 21 upregulated DEGs and 27 downregulated DEGs overlapped between the sexes.

To evaluate top regulated genes by sex in repopulated versus resident microglia with and without injury, we generated volcano plots to establish fold change to significance comparisons (Figure 3b and Supplemental Figure 6). We noted that *Apoe*, previously implicated in microglial phenotypic responses to injury,(21) was highly upregulated in the Injured-Repopulated microglia in both sexes when compared to Injured-Resident microglia. We highlighted additional genes in volcano plots that were highly differentially expressed in Injured-Repopulated microglia or have been previously implicated in the context pain (Figure 3b, red text). Highly regulated female-specific genes included *Septin2*, *Syt11*, and *Atf2*, all of which were downregulated in Injured-Repopulated microglia. Highly regulated male-specific genes included *Csf1r*, *Khdrbs3*, *Fscn1* (all downregulated) as well as *Tlr2*, *Slc2a6*, *Axl* and *Cxcl13* (all upregulated). Highly regulated genes shared between the sexes included: *Serpinf1* (downregulated), as well as *Oas2*, *Cd72*, *Ms4a7* and *Cd300lf* (upregulated) (Figure 3b, red text).

We next performed gene ontology (GO) term analysis on the DEGs from each comparison to identify biological pathways most strongly represented. In the female Injured-Repopulated microglia versus Injured-Resident microglia comparison (pain resolution context), several GO terms related to responses to stress/external stimulus and regulation of cell component organization were detected, as well as "negative regulation of cell activation" (Figure 3c and Extended Data 2). In the male Injured-Repopulated microglia versus Injured-Resident microglia comparison, immune system processes were highly represented as were defense responses and responses to external stimuli/cytokines (Figure 3d and Extended Data 3). We next took all overlapping DEGs from male and female Injured-Repopulated microglia versus Injured-Resident microglia comparisons and ran GO analysis on these shared genes. (Figure 3e and Extended Data 4). While

broad GO terms remained highly represented (defense response, immune system processes, response to external stimulus), we also identified terms related to more specific pathways including "negative regulation of MyD88-dependent TLR signaling pathway" and "regulation of tumor necrosis factor production", consistent with known microglial injury responses.(8) Taken together, this differential gene expression analysis highlights that repopulated microglia are transcriptionally responsive to injury with both sex-specific and sex-distinct gene changes while the behavioral phenotype (i.e. pain resolution) is similar between sexes.

Construction of an unbiased gene co-expression network allows for discovery of novel genes contributing to pain resolution

While the DESeq2 analysis allowed us to identify individual differentially expressed genes, we next sought to discover gene co-expression networks strongly associated with Injured-Repopulated microglia, and therefore pain resolution. To do this, we performed weighted gene co-expression network analysis (WGCNA), which clusters densely interconnected genes into modules in an unbiased manner (Supplemental Figure 7 and 8), without the use of *a priori* knowledge. Importantly, all gene expression changes are used in WGCNA, regardless of strength or directionality, which allows better prediction of integral pathways associated with the cell state analyzed. Forty-four unique modules were defined in females (Figure 4a, c) and 54 unique modules were defined in males (Figure 4b, c). Once these gene modules were constructed, the module eigengenes (ME), the first principal component of each module's expression matrix, were then correlated by sex to each of the 4 trait comparisons to define significant module-trait relationships (Figure 4a-b, also see Extended Data 5 for full list of correlation coefficients and *p*-values by trait). Notably, the Uninjured-Repopulated microglia to Uninjured-Resident microglia comparison, representing the repopulated microglia trait, had 28 significant modules in males and 13 significant modules in females (Figure 4c), indicating networks of genes that distinguish repopulated microglia from resident microglia.

To identify gene clusters strongly associated with pain resolution (Injured-Repopulated microglia to Injured-Resident microglia comparison), we selected modules of interest for further analysis based on a combination of their absolute trait correlations across the 4 trait-comparisons (Figure 4a and b) and the number of differentially expressed transcripts (DETs) from the DESeq2 analysis represented in each module. We thus selected four modules [female: *steelblue* and *violet;* male: *darkseagreen1* and *turquoise*], all of which had a strong correlation to the Injured-Repopulated versus Injured-Resident trait comparison (Figure 4a-b, arrows) and had high percentages of DETs represented (Extended Data 6). To define highly represented biological processes and pathways, GO analysis and Ingenuity Pathway Analysis (IPA) were performed on all transcripts within each module, and genes highly impacting these pathways were further identified. Finally, we established the top 20 genes within each module with the highest gene significance vs. module membership, a measure of the strength of the correlation of the individual gene with the module eigengene (Figure 5). These genes were central to module construction because they correlated with a large number of genes within the module, acting as a major node, and thus serve as natural candidates for further investigation (Figure 5).

For the female *steelblue* module we identified GO terms related to 'response to stress' consistent with identified IPA pathways 'LXR/RXR and FXR/RXR activation' (*Rxry*, *Apoe, Il1rn*) which affect lipoprotein clearance and cholesterol homeostasis and 'purine-nucleoside salvage/degradation pathways' (*Pnp*) which may alter extracellular levels of purine bases, such as adenosine, known to impact antinociception in neurons (Figure 5a and Extended Data 7).(28, 29) The semaphorin 4D receptor, *Cd72*, involved in microglial-mediated CNS inflammation,(30, 31) was identified as a top 20 gene with high gene significance in the *steelblue* module (Figure 5b, c). Regulation of plasma lipoprotein levels was also highly represented by GO analysis and IPA included 'IL-12 signaling' pathway (*Apoe, Prkca)* (Figure 5a and Extended Data 7). For this module, all 5 transcripts for the *Apoe* gene demonstrated positive significance (Figure 5b, c). Finally, antigen processing/presentation (MHCII) pathways were highly represented by GO and IPA, including 'antigen presentation pathway' (*H2-Ab1*, *Cd74*), indicating the Injured-Repopulated microglia are in an active state, surveilling and responding to their environment.

In the female module containing the highest number of DETs, *violet*, several GO terms identified were similar to *steelblue*, including 'response to stress', 'regulation of plasma lipoprotein levels', and 'antigen processing/presentation' (Figure 5d). Interestingly, *violet* also had a high representation of the GO term 'response to stimulus' with related IPA pathways including 'activation of IL-22/IL-10 signaling' (*IL-10Rβ*, *Stat3*), a pathway related to anti-inflammatory effects in microglia and neuroprotective effects of IL-10 following injury (Figure 5d-f and Extended Data 7).(32, 33) Additionally, 'phagosome maturation' (*Cybb*, *Ctsb*) was identified by IPA, an essential process following phagocytosis of debris/apoptotic cells (Extended Data 7). In line with this, a natural candidate identified in the *violet* module,*Cd300lf*, enhances phagocytosis(34) (Figure 5e, f), and may enable Injured-Repopulated microglia to clear neuronal debris following injury.

In the male module *darkseagreen1*, significantly enriched GO terms (Figure 5g) were related to 'regulation of protein transport' and 'protein localization' with related enriched IPA pathways of 'calcium signaling' (*Arcan3*, *Prkaca*, *Asph*), which can change protein location within the cell(35) and 'biosynthesis of phosphatidylcholine and choline' (*Pcyt1a*), whose levels determine physical properties that affect fluidity and protein localization of the cell membrane (Figure 5g, Extended Data 7). One top 20 gene identified in *darkseagreen1* was *Prkaca*, which encodes the catalytic subunit of protein kinase A. Other GO terms enriched related to pre-mRNA processing (*Wdr33*), which directly controls translation in the cell. Another top 20 gene found in this module was *Maf1*, a transcriptional regulator (Figure 5h, i). Overall, the module *darkseagreen1* emphasizes that these Injured-Repopulated microglia are active; tightly regulating protein expression, localization, and function in the cell.

In the male *turquoise* module, GO terms identified included 'immune system process' with IPA pathways such as 'neuroinflammation signaling' (*Irf7, Tlr2, Tnf, Cybb, Ccl2, Ccl5, IL12*) and 'TREM1 signaling' (*Cd40, Itgax, Casp1, IL18, IL1β*). In addition, the male *turquoise* module had several of the same GO terms identified in the female modules of interest, including 'response to stress' and 'response to stimulus' (Figure 5j). Similar to the female *steelblue* module, male *turquoise* was enriched for the GO term 'response to stress' and related IPA pathway 'LXR/RXR activation' (*Rxry*, *Apoe*, *Cd36,*

Il1rn). Similar to the female *violet* module, male *turquoise* was enriched for the GO term 'response to stimulus' and related IPA pathway 'phagosome maturation' (*Cybb, Ctss, Ctsh, Lamp1, Rab7*). Specifically, the genes represented in this pathway related to late phagosome maturation when lysosomal fusion forms the phagolysosome. Interestingly, one of the top 20 genes in this module was *Gm2a*, a gene encoding a co-factor of lysosomal enzymes. Further, two cathepsins (*Ctss* and *Ctsh*) with relevance to pain (36) were in the top 20 gene list in *turquoise*. These proteins are enriched in actively phagocytic cells, have lysosomal activity, and modify neuronal spine density extracellularly.(37) The *turquoise* module captures several biological functions similar to those identified in the female modules of interest, pointing towards a sex-independent phenotype of repopulating microglia active in phagocytosis and stress responses.

To compare the shift in gene expression in males and females captured by the WGCNA modules of interest, we plotted the fold change of transcripts from our selected modules in the Injured-Repopulated versus Injured-Resident microglia comparison (Supplemental Figure 9a) and observed a strong correlation between sexes (r = 0.8680). In contrast, when the fold change comparison was expanded to include all transcripts expressed in both sexes (Supplemental Figure 9b), there was very little correlation (r = 0.1581). This suggests that WGCNA identified a shared transcriptomic shift in repopulated microglia in both males and females that may contribute to the pain resolution phenotype observed.

Human dorsal horn spinal microglia exhibit heterogeneous cell states

Since our overall goal was to identify microglial targets for pain relief in humans, we next isolated human spinal cord dorsal horn microglia to cross-reference their transcriptomes with the generated mouse datasets. We performed single nuclei RNA sequencing (snRNAseq) on nuclei isolated from lumbar spinal cord from either a male or female post-mortem human donor with no known pain history (Supplemental Table 2). We isolated dorsal horn nuclei and enriched for microglia using negative selection sorting to provide an unbiased sample of microglia nuclei for sequencing (Figure 6a). The male and female snRNAseq datasets were then integrated and UMAP projection of the 6,591 nuclei revealed 7 clusters representing unique cell types. These clusters were defined using a human brain DropNc-seq dataset,(38) and included microglia, oligodendrocytes, oligodendrocyte precursor cells (OPCs), astrocytes, endothelial cells, neurons, and neuronal stem cells (NSCs) (Figure 6b and 6c). The negative selection strategy enriched microglial nuclei to ~40% of the sample, compared to ~3.7% collected from whole mouse spinal tissue in other studies(39) (Figure 6b). Microglial nuclei clusters expressed known marker genes described in previous studies including *ITGAM*, *CTSS*, *CSF1R* and *C1QA* (Figure 6d).(21) One small nuclei cluster in the upper-left quadrant of the UMAP was determined to have high expression of T cell markers (and lacking microglial gene expression) and subsequently eliminated before further sub-clustering of microglia (Figure 6c and d). A total of 2,316 microglial nuclei (dashed box in Figure 6c) were re-clustered using oh wow,(40) revealing 6 distinct microglia sub-clusters based on unique gene expression profiles (Figure 6e, Supplemental Table 3, and Extended Data 8). GO analysis was then used to identify microglia sub-cluster cell states (Figure 6f and Extended Data 9). As expected from human post-mortem tissue, we detected a small cluster, cluster 6 (97 nuclei) of dying microglia with a top GO term "cell death". We also

detected a small cluster, cluster 5 (81 nuclei), that represented proliferative microglia with top terms such as "cell cycle", "DNA metabolic processes", and "chromosome organization". Notably, cluster 5 expressed cluster-unique gene *MKI67* (p-value adj = 6.02E-134), the gene encoding Ki-67, as well as *TOP2A* and *POLQ*, each prominent markers of proliferation (Supplemental Figure 10a and Extended Data 8). We identified an additional sub-cluster, cluster 4 (81 nuclei), with a signature similar to reactive microglia with GO terms such as "cell activation", "regulation of cell motility", and a cluster-unique term "inflammatory process", with key genes significantly expressed such as *TLR2* and *CYBB* (also known as *NOX2*), both potent neuroinflammatory-associated genes expressed by microglia(41, 42) (Supplemental Figure 10b). Additionally, a top differentially expressed gene in cluster 4 was AC083837.1 (p-value adj = 1.17E-100), a novel long noncoding RNA induced in the human microglial cell line (HMC3) in response to LPS treatment(43) (Supplemental Figure 10b). Importantly, we further identified a large nuclei cluster that represented homeostatic microglia (cluster 1, 730 nuclei), with cluster-unique terms "myeloid cell homeostasis" and "regulation of supramolecular fiber organization" as well as "regulation of cell adhesion" and "cell junction organization". Anti-inflammatory or homeostatic genes such as *TGFBI*, *ITGAX*, and *IGF1R*, were significantly expressed with positive fold-changes, while inflammatory-associated genes such as *TLR2* and *CYBB* had negative fold-changes in homeostatic cluster 1 compared to other clusters (Supplemental Figure 10b-c and Extended Data 8). The final two clusters (cluster 2, 857 nuclei; cluster 3, 470 nuclei) had both homeostatic and reactive features with terms shared by homeostatic cluster 1 such as "immune system process" and "regulation of cell adhesion" in addition to terms shared by clusters 4 and 6 such as "cell activation" and "cell death" (Figure 6f).

Identification of human-relevant homeostatic gene targets detected in repopulated mouse microglia

To identify human-relevant microglia-expressed genes found in our Injured-Repopulated microglia vs Injured-Resident microglia mouse dataset, we first selected mouse genes that met a DESeq2 cutoff of -log10(p-adjusted) > 1.3 and log2(fold change) > |0.4| and were within our top WGCNA modules of interest. We next categorized these top mouse genes as having either sex-independent or sex-specific expression. The resulting mouse gene list contained 11 female-specific genes, 30 male-specific genes, and 21 overlap genes (Supplemental Table 4). These mouse genes were then screened across the human microglial nuclei clusters to identify cluster-specific expression patterns. Twenty-two of these mouse genes were significantly differentially expressed across the human microglia clusters (p-value<0.01) (Figure 6g). We identified one gene, *KHDRBS3* (also known as *SLM2*) that had significantly lower expression specifically in homeostatic human cluster 1, and was also down-regulated in mouse Injured-Repopulated microglia. Additionally, six genes (*CD300LF, CD72, TGFBI, GM2A, LAMP1,* and *SAMD9L*) had significantly higher expression in homeostatic human cluster 1, and no other cluster (Figure 6g-h and Supplemental Figure 10c). Interestingly, all these genes were upregulated in mouse Injured-Repopulated microglia (Supplemental Table 4), indicating possible involvement in homeostatic functions in humans and thus may serve as relevant microglial targets to promote spinal cord homeostasis and pain resolution.

Discussion

In this study, we established the importance of microglia at multiple time points after pain-producing peripheral injury, identified transcriptomic signatures of spinal cord microglia associated with a pain-resolved state, and screened top gene candidates with those expressed by microglial subclusters obtained from human spinal cord transcriptional profiling. We applied a genetic depletion strategy using Cx3CR1-Cre$^{ERT2-eYFP}$;R26-iDTR^{LSL} mice to temporally and selectively deplete microglia without affecting peripheral circulating monocytes/macrophages.(8, 13) We find that depletion of microglia at the acute-to-chronic pain transition (at 3-week post-injury) is sufficient to resolve existing allodynia and thermal hyperalgesia in both sexes. Importantly, the onset of pain resolution coincided with spinal cord microglial repopulation, not microglial depletion. To identify a potential "pro-resolution" gene signature in these repopulated spinal cord microglia, we performed RNA sequencing followed by bioinformatic analysis using DESeq2 and WGCNA. WGCNA is a powerful technique that has historically been applied to population-level studies of publicly available datasets.(44, 45) Our study is unique in applying WGCNA in the context of pain transcriptomic analysis of microglia. Using this in-depth, unbiased approach, we identify both sex-dependent and independent microglial transcriptional signatures related to the uninjured, injured, or pain-resolved states. Given the limitations of using mice as a model for human disease, we next generated a snRNA-seq dataset from human lumbar spinal cord grey matter negatively-selected microglial nuclei. We detected heterogeneity of microglia in this anatomically limited region including 6 subclusters with unique transcriptomes, some of which shared similarities with previously identified subpopulations in brain.(46) Finally, we cross-referenced candidate mouse microglial genes linked to the pain-resolved state with this human snRNA-seq dataset and identified genes of high translational interest based on their sub-cluster expression profiles.

Microglia are associated with the acute phase/initiation of pain after peripheral injury(2); our data using genetic microglial depletion suggests they may also contribute to the transition from acute-to-chronic pain, and perhaps even to pain resolution. Previous studies have demonstrated that microglial activation is necessary(5) and sufficient(47) to initiate acute pain. Microglial depletion studies using pharmacologic or genetic tools show that microglia also contribute to initiation of pain progression in models of nerve injury(10-12). We find that preventive depletion of microglia (at the time of injury) was insufficient to completely reverse allodynia. However, the extent of improvement was similar in magnitude to that observed after early microglial depletion in a high-frequency stimulation model of pain(2) and in spinal nerve transection.(12) This lack of full recovery may be due to nociceptor hyperactivity or high levels of acute nociceptor-derived inflammatory signals acting on the spinal cord environment immediately post-injury.(48) Of note, consistent with our own findings, several studies(2, 12, 49, 50) reported equivalent improvements in pain outcomes in both sexes with microglial manipulation. Taken together, this suggests that microglia themselves are unlikely to be sex-specific contributors to pain progression, but rather microglial expressed receptors(8, 51) or chemokines(2) may be sex-specific.

The current work temporally extends the involvement of microglia to the acute-to-chronic phase, with microglial depletion at 3 weeks post-injury significantly and persistently improving pain trajectory to baseline levels. In agreement, myeloid cell

465 depletion with the CSF1 inhibitor PLX5622 at 28-days post-peripheral nerve injury
466 reversed mechanical and cold allodynia.(52) In contrast, Peng et al.(12) demonstrated that
467 early depletion of microglia delayed development of allodynia, while late depletion of
468 microglia only transiently improved allodynia. The reason for this discrepancy may relate
469 to the type of pain model used (direct nerve injury vs. fracture/immobilization), or exact
470 timing of microglial depletion (Day 7 post-injury vs. Day 21 post-injury). In contrast to
471 the commonly used nerve injury models,(53, 54) the tibial/fracture model of CRPS
472 exhibits a clearly timed transition from acute-to-chronic pain, and triggers both
473 inflammatory and neuropathic mechanisms, mimicking the clinically relevant human
474 condition.(25, 55)
475 In our study, pain resolution after microglial depletion at the acute-to-chronic
476 phase coincided with the timeframe of complete repopulation of CNS microglia. This
477 outcome suggests that repopulated microglia may re-establish homeostasis within the
478 pain circuit. Indeed, newly repopulated microglia can function to repair synapses in the
479 hippocampus as well as promote recovery following brain injury(56, 57). These cells also
480 retain the ability to respond to environmental cues and our WGCNA analysis highlights
481 that they remain highly active cells engaged in surveillance and phagocytosis.(58, 59)
482 The possibility that repopulated microglia exhibit a phenotype that is distinct from
483 homeostatic microglia is further supported by transcriptome analyses showing clear
484 differences between repopulated and "control" brain microglia.(24, 59) Similarly, the
485 transcriptomes of repopulated spinal microglia were distinct from resident microglia in
486 this study. Furthermore, the environment (either injured or uninjured) in which microglia
487 repopulate also influences microglial phenotype. Perhaps not surprising given that
488 microglia are dynamic, multidimensional cells constantly surveying their environment
489 and responding to stimuli with a range of state changes.(60, 61) An urgent question
490 remains regarding whether these heterogenous microglial states may have functional
491 significance in disease progression, or resolution, in particular for pain.
492 Since microglia repopulation did not result in re-sensitization of the periphery,
493 and repopulated microglia were morphologically distinct from control microglia, our
494 model allowed for identification of genes with potential to contribute to pain resolution.
495 The intriguing possibility that specific populations of microglia may contribute to pain
496 resolution is supported by a seminal study characterizing CD11c+ spinal cord microglia
497 as necessary and sufficient to the resolution of pain after peripheral nerve injury in both
498 sexes.(50) Aside from high expression of *Itgax*, *Igf1* and *Apoe*, this antinociceptive
499 subpopulation also highly expressed the receptor tyrosine kinase, *Axl*. Importantly, we
500 also find upregulation of *Apoe* (see below) and *Axl* in both male and female microglia
501 isolated from the pain resolution group. Upregulation of *Apoe* in brain microglia has been
502 detected in multiple disease states including Alzheimer's disease,(62) and multiple
503 sclerosis.(63) Of particular relevance, in a model of neuropathic pain *Apoe* was
504 upregulated in spinal cord microglia in both sexes post-injury.(21) The strongest
505 expression of *Apoe* was in the single-cell cluster that had axon tract-associated microglia
506 (ATMs) and disease-associated microglia (DAM) signatures, previously identified in
507 diseased brain microglia.(46) In partial agreement with these findings, we detected
508 multiple *Apoe* transcripts upregulated (though not significantly) in resident microglia in
509 both sexes following injury, however, we observed significant upregulation of *Apoe* in
510 repopulated microglia in the pain resolution group. While *Apoe* is a gene of interest due

511 to its top-ranking expression pattern in multiple contexts, its presence in a diversity of
512 microglial states, spanning reactive to resolving, suggests the gene may in fact be a
513 marker for highly active rather than disease-promoting microglia, especially in the
514 context of pain. In support of this interpretation, we detected widespread expression of
515 *APOE* in our human microglial nuclei clusters, a finding supported by a recent human
516 spinal cord sequencing study.(64) Additional studies directly testing the function of *Apoe*
517 in microglia in the context of pain will be necessary to implicate it as a pain-regulating
518 gene.
519 For translatable therapies to be developed, it is necessary to validate mouse-
520 identified gene targets using human tissue samples. To address this, we profiled single
521 nuclei of human spinal microglia taken specifically from the lumbar grey matter (dorsal
522 horn). We thus focused on microglia in a pain-relevant circuit, crucial given that gene
523 signatures and cellular states are defined by microglial environment.(22, 65, 66) We
524 performed negative selection (removing astrocytes, neurons, and oligodendrocytes) to
525 enrich the sample 10-fold for microglia, while also capturing those not expressing
526 canonical positive-selection markers (ex. Iba1 or Cx3CR1). This enhanced our ability to
527 characterize human microglial states, which are known to be more heterogeneous
528 compared to other species including the mouse.(67) Using this region-specific, negative-
529 selection approach, we uncovered 6 microglial clusters that were spatially distinct by
530 UMAP and displayed unique gene expression patterns. Of note, we observed one large
531 spatially distinct cluster by UMAP (cluster 1) that contained homeostatic gene expression
532 signatures and lacked reactive ones.
533 To concentrate our gene identification to those with human-relevance, we
534 screened top candidate mouse genes for expression within human microglia clusters. We
535 identified several genes significantly upregulated in repopulated mouse microglia from
536 the pain resolution group, also significantly, and specifically, expressed by human
537 homeostatic cluster 1. *CD300LF* (the human counterpart of the mouse gene *cd300f* which
538 is a perfect functional ortholog(68)) encodes a member of the CD300 cell surface
539 glycoprotein family that function to positively regulate phagocytosis of apoptotic cells, a
540 function increased in a spinal dorsal horn microglia subpopulation shown to promote pain
541 resolution following injury.(34, 50) Specifically, *CD300LF* is an inhibitory receptor for
542 myeloid cells that negatively regulates TLR signaling via MYD88.(69) In addition, over-
543 expression of *CD300LF* has a neuroprotective effect after acute brain injury,(70) and
544 microglia isolated from mice resistant to cerebral malaria express high levels of *cd300lf*
545 and inhibit inflammation.(71) Another gene identified was *CD72*, whose protein product
546 is a receptor for semaphorin 4D and contributes to microglial-mediated CNS
547 inflammation.(30, 31) Lastly, we identified *GM2A*, which encodes a small, secretable
548 glycolipid transport protein and stimulates the degradation of ganglioside GM2 in the
549 lysosome. Elevated levels of GM2A in culture reduces neurite extension and neuronal
550 firing rate, which in the context of pain and dorsal horn circuitry, may be beneficial.(72)
551 In this study, we took advantage of a pain resolution context to profile
552 repopulated spinal cord microglia and identify genes that may promote homeostatic
553 features of microglia, and ultimately promote pain recovery after injury. Future studies
554 will evaluate whether these repopulated microglia directly contribute to the resolution of
555 pain, similar to previously described CD11c+ microglia,(50) or whether simply the
556 absence of reactive microglia in a short time window prevents chronic pain in our

depletion studies. Our findings, that repopulated microglia are transcriptomically active, express markers overlapping with human homeostatic microglia, and are distinct from resident microglia, suggest they contribute in a unique manner to the spinal cord circuit environment in the weeks following injury. Interrogating the individual genes identified in this study, many of which have no known function in microglia, will be an exciting next step to confirm their potential as therapeutic targets for analgesic development.

Materials and Methods

Animals

Adult male and female mice 10-12 weeks old at the start of the experiments were housed 2-5 per cage maintained on a 12-hour light/dark cycle in a temperature-controlled environment with *ad libitum* access to food and water. Male mice weighed approximately 25 g at the start of the study, and female mice weighed approximately 20 g at the start of the study. Mice used in this study: wild type C57BL/6J mice (Jax stock #00664), $CX_3CR1^{CreERT2\text{-}EYFP}$ (Jax stock #021160),(13) Rosa26-loxP-stop-DTR ($R26^{iDTR}$, Jax stock #007900). To specifically and conditionally ablate central CX_3CR1 cells (microglial depletion), we crossed homozygous $CX_3CR1^{CreERT2\text{-}EYFP}$ with homozygous $R26^{iDTR/iDTR}$ mice to generate double heterozygous Cx3CR1-$Cre^{ERT2\text{-}eYFP}$;R26-$iDTR^{LSL}$ mice. Mouse genotypes from tail samples were determined using real time RT-PCR with specific probes designed for each gene (Transnetyx, Cordova, TN). Control subjects for all behavioral studies were mice without the $R26^{iDTR}$ allele: Cx3CR1-$Cre^{ERT2\text{-}eYFP}$; R26-$iDTR^{+/+}$ that received tamoxifen (TAM) and diphtheria toxin (DT) with the same dosing and administration schedule as experimental mice.

Drugs and Route of Administration

Tamoxifen (Sigma, #T5648) was dissolved in corn oil at a concentration of 25 mg/mL. Mice were injected intraperitoneally (i.p.) at 100 mg/kg daily for 5 days. Diphtheria toxin (DT) from *Corynebacterium diphtheriae* (Sigma, #D0564-1MG) was dissolved in sterile water to a concentration of 10 µg/mL and 0.1 mL (1000 ng) was administered i.p. daily for 3 days.

Tibial fracture/casting model of complex regional pain syndrome (CRPS)

Mice were anesthetized with isoflurane and underwent a closed right distal tibia fracture followed by casting. The right hind limb was wrapped in gauze and a hemostat was used to make a closed fracture of the distal tibia. The hind limb was then wrapped in casting tape (ScotchCast™ Plus) from the metatarsals of the hind paw up to a spica formed around the abdomen to ensure that the cast did not slip off. The cast over the paw was applied only to the plantar surface with a window left open over the dorsum of the paw and ankle to prevent constriction when post-fracture edema developed. Mice were inspected throughout the post-operative period of cast immobilization to ensure that the cast was properly positioned. At 3 weeks post-fracture, mice were briefly anesthetized, and casts were removed with cast shears. For behavioral assessment, mice were tested beginning three days after cast removal at 3 weeks until 9 weeks post-fracture, as indicated in each section below. CRPS model generation and behavioral testing were conducted following well established methods for evaluating mouse behavior in the tibial fracture-casting model of CRPS.(73, 74)

Behavioral testing

To ensure rigor in our findings and avoid the contribution of experimenter sex to our behavioral data, experimenters were female or there was a female scientist's lab coat in the room during acclimation and testing.(75) *In vivo* behavioral testing was performed in a blinded fashion. All testing was conducted between 7:00 am - 1:00 pm in an isolated, temperature- and light-controlled room. Mice were acclimated for 30 - 60 minutes in the

testing environment within custom clear plastic cylinders (4” D) on a raised metal mesh platform (24” H). Mice were randomly placed in a cylinder; after testing, mouse identification numbers were recorded on the data sheet.

Mechanical nociception assays

To evaluate mechanical reflexive hypersensitivity, we used a logarithmically increasing set of 8 von Frey filaments (Stoelting), ranging in gram force from 0.007 to 6.0 g. These were applied perpendicular to the plantar hind paw with sufficient force to cause a slight bending of the filament. A positive response was characterized as a rapid withdrawal of the paw away from the stimulus filament within 4 s. Using the up-down statistical method,(76) the 50% withdrawal mechanical threshold scores were calculated for each mouse and then averaged across the experimental groups. Mechanical nociception testing was performed at Weeks 3, 5, 7, and 9 post-fracture.

Paw Edema, Unweighting and Temperature Measurements

Hind paw edema was determined by measuring the hind paw dorsal-ventral thickness over the midpoint of the third metatarsal with a LIMAB laser measurement sensor (LIMAB, Goteborg, Sweden) while the mouse was briefly anesthetized with isoflurane. Temperature and hind paw thickness data were analyzed as the difference between the fracture side and the contralateral intact side and averaged across experimental groups. Paw edema was measured at 4 weeks post-fracture.

An incapacitance device (IITC Inc Life Science, Woodland Hills, CA) was used to measure hind paw unweighting. Mice were manually held in a vertical position over the apparatus with the hind paws resting on separate metal scale plates, and the entire weight of the mouse was supported on the hind paws. The duration of each measurement was 6 seconds, and 6 consecutive measurements were taken at 60-second intervals. Six readings were averaged to calculate the bilateral hind paw weight-bearing values. Unweighting was measured at baseline and then again at 4 weeks post-fracture. Data was analyzed as a ratio between the right hind paw weight divided by the sum of right and left hind paw values $[2R/(R + L)] \times 100\%$).(77)

The temperature of the hind paw was measured using a fine-gauge thermocouple wire (Omega, Stamford, CT). Temperature testing was performed over the hind paw dorsal skin between the first and second metatarsals (medial), the second and third metatarsals (central), and the fourth and fifth metatarsals (lateral). The measurements for each hind paw were averaged for the mean paw temperature. Data were expressed as the average difference between the ipsi- and contralateral hind paw within an experimental group. Paw temperature was measured at 4 weeks post-fracture.

Thermal nociception assays

To evaluate thermal-induced reflexive responses, we used the hotplate test (plate temperature was set to 52.5°C). Mice were placed on the plate and the latency (seconds) to the first appearance of a reflex response (flinch) was recorded as a positive reflex withdrawal response. A maximal cut-off of 45 s was set to prevent tissue damage. Only one exposure to the hotplate was applied on a given testing session to prevent behavioral sensitization that can result from multiple noxious exposures. Measurements were made at 5 weeks post-fracture.

657
658 **Immunohistochemistry**
659 Mice (12 – 30 weeks) were transcardially perfused with 10% formalin in PBS.
660 The spinal cord (lumbar cord L3 - L5 segments) were dissected from the mice and
661 cryoprotected in 30% sucrose in PBS and frozen in O.C.T. (Sakura Finetek, Inc.). Spinal
662 cord sections (40 µm) were prepared using a cryostat (Leica Biosystems) and incubated
663 in blocking solution (5% normal donkey serum and 0.3% Triton X-100 in PBS) for 1 h at
664 room temperature followed by incubation with primary antibodies at 4°C, overnight. The
665 following primary antibodies were used: rat anti-CD11b (Bio-Rad, #MCA711G, 1:500),
666 and rabbit anti-Iba1 (Wako, #019-19741, 1:500). Tissues were washed with 1X PBS 3
667 times and sections were incubated with appropriate secondary antibody conjugated to
668 AlexaFluor in 1% normal donkey serum, 0.3% Triton X-100, and 1X PBS for 2 h at room
669 temperature. Sections were mounted with Fluoromount G with DAPI medium
670 (ThermoFisher, #00-4959-52). Images were collected with a Keyence BZ-X800
671 fluorescent microscope (Keyence) using the sectioning module to remove non-focused
672 light using 20x (NA 0.75) or 60x (NA 0.95) objectives. Four to five lumbar spinal cord
673 dorsal horn sections were counted and averaged for 2-3 mice per group.
674
675 **Sholl analysis for microglial morphology**
676 Lumbar spinal cord was sliced on a cryostat at 40 µm and microglia were labeled
677 by immunohistochemistry using the rabbit anti-Iba1 antibody (Wako, #019-19 741,
678 1:500). Dorsal horn localized microglia were imaged using a Keyence BZ-X800
679 fluorescent microscope (Keyence) using the sectioning module (1D Slit method) to
680 remove non-focused light using a 40X objective. Each z-stack was taken at the same
681 exposure using 43 slices with a 0.3 µm step size. Images were imported into ImageJ/FIJI
682 and maximum intensity projections of dorsal horn images were generated. Region of
683 interest (ROI) was selected around individual microglia. Unsharp Mask was applied
684 using set radius to 3 pixels and weight of 0.6 followed by the de-speckle tool was to
685 remove non-specific background. The images were made binary and 'remove outliers'
686 was used at threshold of 50. The Eraser tool was then used to manually eliminate Iba1+
687 processes within the frame that were clearly not associated with the microglial cell
688 analyzed. Between 37-92 microglia per animal per time-point (Baseline: 185 microglia,
689 Day 1: 74 microglia, Day 3: 117 microglia, Day 14: 87 microglia) were analyzed by
690 Sholl analysis plugin in ImageJ/FIJI with a start radius of 0.5 µm and a step size of 1 µm.
691
692 **Statistics for behavioral paradigms and Sholl analysis**
693 Cohort sizes were determined based on historical data from our laboratory using a
694 power analysis to provide >80% power to discover 25% differences with $p<0.05$ between
695 groups to require a minimum of 4 animals per group for all behavioral outcomes, and 2
696 animals per group for Sholl analyses with >30 microglia counted per animal per time-
697 point. All experiments were randomized by cage and performed by a blinded researcher.
698 Researchers remained blinded throughout histological, biochemical, and behavioral
699 assessments. Groups were unblinded at the end of each experiment before statistical
700 analysis. Data are expressed as the mean ± SEM. Statistical analysis was performed using
701 GraphPad Prism version 8.4.1 (GraphPad Software) or R, as described in Methods. Data
702 were analyzed using a Student's t tests, or ordinary one-way with Dunnett's or Tukey's

post-hoc test, or two-way analysis of variance with a Bonferroni post-hoc test, as indicated in the main text or figure captions, as appropriate, with complete statistical analyses detailed in Table. The "n" for each individual experiment is listed in the figure legends.

Spinal Cord Cell Dissociation

Mice were anesthetized with 120 mg/kg ketamine and 5mg/kg xylazine and perfused with 15 mL ice-cold Medium A (50 mL 1x HBSS without Ca2+ or Mg2+ (Gibco, 14185052), 750 µL 1M HEPES (Gibco, 15630080), 556 µL 45% glucose (Corning, 25-037-CI)). Lumbar spinal cords were isolated and placed in 2 mL Medium A + 80 µL DNase I (12,400 units/mL, Sigma, 11284932001) until all samples were dissected. Samples were dounce-homogenized, passed through a 100 µm strainer, washed with 5 mL Medium A, and spun down by centrifugation at 340 x *g* for 7 minutes at 4°C. Supernatant was removed, and pellets were resuspended in 6 mL 25 % Standard Isotonic Percoll (Percoll: GE Healthcare, 17-5445-02 with 10% 10x PBS) in Medium A. The suspension underwent centrifugation for 20 minutes at 950 x *g* at 4°C to remove myelin. Supernatant was discarded then washed with 5 mL Medium A and spun down by centrifugation at 340 x *g* for 7 minutes at 4°C. Cells were resuspended in FACS buffer (5 mM EDTA in 1% BSA in 1x PBS).

Flow Cytometry

The following antibodies were used for flow cytometry: e450-conjugated anti-CD3 (eBioscience, #48-0031-82), e450-conjugated anti-CD19 (eBioscience, #48-0193-82), PE-Cy7-conjugated anti-CD45 (Biolegend, #103114), APC-conjugated anti-CD11b (Biolegend, #101212). Dead cells were stained with 1:1000 SYTOX Blue (Invitrogen, #S34857). Cell suspension was then spun down at 300 x *g* for 5 minutes at 4°C. The FACS buffer supernatant was suctioned off, and cells were resuspended in fresh FACS buffer. Before staining, all samples were pre-blocked with 1:100 anti-CD16/CD32 (BD Pharmingen, #553142) for 5 minutes at room temperature. Afterward, all antibodies were added to the samples at 1:100 along with 1:1000 Sytox Blue and placed on ice for 30 minutes. Samples were spun down for 5 minutes at 400 x *g* at 4°C, suctioned and replaced with fresh FACS buffer. Suspension was then spun down for 5 minutes at 400 x *g* at 4°C. Supernatant was suctioned off, then cells were again resuspended in FACS buffer and passed through 35 µm filter into polystyrene tubes. Samples were sorted using a BD Aria II (BD Biosciences). Flow cytometry analysis was done using FlowJo v10.6.2. Single cells were gated for live (SYTOX blue negative), CD19- CD3- $CD45^{mid}$ then $CD11b^{+}$ and Cx3CR1-YFP^{+} to isolate microglia from spinal cord.

Preparation of samples for sequencing

For male samples, whole RNA was isolated from FACS microglia using the RNeasy® Plus Micro kit (Qiagen, Cat No. 74034) then cDNA was synthesized using the SMART-Seq® v4 Ultra® Low Input RNA kit (Takara Bio USA Inc. Cat No. 634888). Libraries were prepared using the Nextera™ DNA Flex Library Prep (Illumina Cat No. 20015828) and sequencing performed by the Stanford Genomics Service Center on a HiSeq4000 using a paired end 2x150bp unstranded protocol. For the female samples, microglia were isolated by FACS into Trizol LS (Invitrogen, Cat No. 10296028) and sent

749 to Azenta Life Sciences (formerly Genewiz) to isolate total RNA using a routine protocol
750 with glycogen added in the precipitation step followed by sequencing on an Illumina
751 HiSeq using paired end 2x150bp unstranded protocol.
752
753 **DESeq2 analysis**
754 Raw sequencing data was analyzed using the nf-core/rnaseq v3.5 RNA-Seq
755 analysis pipeline (https://nf-co.re/rnaseq)(78) with nf-core helper tools v2.2
756 (https://github.com/nf-core/tools)(78) which was run using STAR and RSEM with
757 isoform (transcript) counts and extensive quality control. The Nextflow v22.01.0
758 workflow tool (https://github.com/nextflow-io/nextflow)(79) facilitated the running of
759 various pipeline tasks across a compute cluster in a very portable manner. FastQC
760 v0.11.9 (https://www.bioinformatics.babraham.ac.uk/projects/fastqc/)(80) was used to
761 run quality control checks on raw FASTQ sequence data. The wrapper tool Trim Galore
762 v0.6.7 (https://www.bioinformatics.babraham.ac.uk/projects/trim_galore/)(81) that
763 employs Cutadapt v3.4 and FastQC v0.11.9 was run to consistently apply quality and
764 adapter trimming to FASTQ files. Alignment to the GENCODE GRCm38 release M25
765 reference was done using STAR v2.7.6a and the aligned transcripts were quantitated by
766 RSEM v1.3.1 (http://deweylab.github.io/RSEM/).(82) MultiQC v1.11
767 (https://multiqc.info/)(83) helped to aggregate results from the various bioinformatics
768 analyses across the many samples into a single report. Differentially expressed transcripts
769 were detected from raw transcript counts produced by the STAR-RSEM pipeline using
770 DESeq2 v1.34.0 (https://bioconductor.org/packages/release/bioc/html/DESeq2.html)(84)
771 running in R v4.1.3.
772
773 **Weighted gene co-expression network analysis**
774 Weighted gene co-expression network analysis (WGCNA) was used to identify
775 clusters (modules) of highly correlated genes. Uninjured-Resident, Injured-Resident,
776 Uninjured-Repopulated, and Injured-Repopulated replicates from female and male mice
777 were analyzed using WGCNA v1.70.3 package in R v4.1.3.(85) Variance stabilization
778 transformed RNA-Seq expression data was loaded and genes and samples with too many
779 missing values, if any, were removed. Samples were then clustered based on their
780 Euclidean distance to see whether there were any obvious outliers. Traits of interest
781 including Uninjured-Repopulated microglia vs. Uninjured-Resident microglia, Injured-
782 Repopulated microglia vs. Uninjured-Repopulated microglia, Injured-Repopulated
783 microglia vs. Injured-Resident microglia, and Injured-Resident microglia vs. Uninjured-
784 Resident microglia were visualized to see how they related to the sample dendrogram. A
785 step-by-step network and module detection approach was then employed. The soft
786 thresholding power to which co-expression similarity was raised to calculate adjacency
787 was chosen based on the criterion of approximate scale-free topology. Adjacencies were
788 calculated based on the chosen soft thresholding power. To minimize effects of noise and
789 spurious associations, the adjacency was transformed into Topological Overlap Matrix
790 (TOM) following which the corresponding dissimilarity was calculated. Hierarchical
791 clustering was employed to produce a dendrogram of genes. The Dynamic Tree Cut R
792 library that implements novel dynamic branch cutting methods was used to detect clusters
793 (modules) of highly co-expressed genes in the dendrogram. Modules whose expression
794 profiles were very similar were merged after calculating eigengenes of modules and

clustering them on their correlation. A cut height of 0.25 corresponding to a correlation of 0.75 was used to merge modules and assign module colors. In the next step modules that were significantly associated with above-mentioned traits of interest such as Uninjured-Repopulated microglia vs. Uninjured-Resident microglia, Injured-Repopulated microglia vs. Uninjured-Repopulated microglia, Injured-Repopulated microglia vs. Injured-Resident microglia, and Injured-Resident microglia vs. Uninjured-Resident microglia were identified by quantifying the module-trait relationships by correlation values and p-values. Next, associations of individual genes with each trait of interest were quantified by defining gene significance (GS) as the absolute value of the correlation between the gene and the trait. For each module, a quantitative measure of module membership (MM) was defined as the correlation of the module eigengene and the gene expression profile which allowed quantification of the similarity of all genes to every module. The GS and MM measures were used to identify genes that have a high significance for each trait of interest as well as high module membership in interesting modules. Finally, a table was created to show gene annotation, module color, gene significance for traits of interest with p-values, and module membership with p-values in all modules.

Gene ontology and signaling pathway analysis of Gene sets

Gene sets of interest were analyzed via the g:profiler website(86) to identify enriched Gene Ontology Terms and KEGG Pathways based on a threshold of Benjamini-Hochberg FDR > 0.05. Gene Ontology terms were visualized with GO-Figure! version 1.0.1(87) utilizing the 2021-02-01 release of the Gene Ontology (10.5281/zenodo.2529950) and the 2022-03-02 release of the UniProt GO Associations.(88) The pathway analysis was executed through the use of QIAGEN IPA (QIAGEN Inc., https://digitalinsights.qiagen.com/IPA).(89)

Isolation of postmortem human microglia nuclei

Human lumbar spinal cord was removed immediately after organs were removed for transplant from either male or female donor (see Supplemental Table S2). The lumbar segment was further dissected into three smaller segments, and immediately frozen on dry ice and stored at -80°C in Eppendorf or conical tubes. Lumbar spinal cord was then embedded in OCT and sectioned at 80 µm thickness (40-50 total sections per sample was used). Dorsal horn was collected by microdissection and immediately homogenized in Nuclei Lysis buffer on ice (10 mM Tris-HCl pH 8.0, 250 mM sucrose, 25 mM KCl, 5 mM MgCl2, 0.1% Triton-x 100, 0.5% RNasin® Ribonuclease Inhibitors (Fisher/Promega, PRN2615), 1X Protease inhibitor, 0.1 mM DTT). Samples were then filtered through a 40 µm nylon cell strainer (BD#352340) pre-wet with Nuclei Lysis buffer in a 15 mL conical tube and another 2 mL of lysis buffer was used to rinse the filter. The homogenate was then centrifuged at 900 × *g* for 10 min at 4°C. The resulting pellet was resuspended in 6 mL of sterile 25% Standard Isotonic Percoll (SIP) to remove myelin and centrifuged at 2000 x *g* for 20 min at 4°C without brake. The myelin layer was discarded and the nuclei pellet was resuspended in 1 mL of Staining buffer (1XPBS, 0.8%BSA, 0.5% RNasin plus). The nuclei suspension was transferred to an Eppendorf tube and centrifuged at 900 × *g* for 10 min at 4°C. Supernatant was discarded and the pellet was resuspended in Staining buffer containing the Human BD Fc Block™ antibody (BD, 564220) and incubated with agitation for 15 min at 4°C in a cold room. Samples

were then incubated with rabbit anti-NeuN Alexa Fluor® 647 (1:1000; Abcam, ab190565), rabbit anti-Sox10 Alexa Fluor® 647 (1:5000; Abcam, ab270151), rabbit anti-Sox9 Alexa Fluor® 555 (1:1000; Millipore, AB5535-AF555), and DAPI (1:1000, ThermoFisher, 62248). Samples were incubated with agitation for 30 mins at 4 °C (protected from light) and centrifuged at 900 × *g* for 10 minutes at 4°C. Samples were then resuspended in 1mL Staining buffer and centrifuged at 900 × *g* for 10 minutes at 4°C. Nuclei were resuspended in 400-500 µl of Staining buffer and filtered through the lid of 35µm BD FACS tube before sorting on a BD Aria II (BD Biosciences) machine. DAPI only positive nuclei were sorted away from nuclei co-positive with any other signal to negatively select for and enrich nuclei sample for microglia. Nuclei were then centrifuged at 200 x *g* for 1 min using gentle brake and acceleration and repeated two additional times. Supernatant was removed to leave ~ 60 µl to resuspend nuclei.

Single-nuclei RNA sequencing

Nuclei were counted on a hemocytometer and estimated nuclei/µl were calculated for loading onto a 10X Genomic Chromium single cell chip (10x Genomics). Reverse transcription and subsequent library preparations were performed using the Chromium Next GEM Single Cell 3′ Kit v3 by the Stanford Functional Genomics Facility per manufacturer's instructions. Samples were then sequenced to an average depth of 97,000-120,000 reads per nuclei on an Illumina NovaSeq6000 sequencer.

snRNA-seq data processing

Cell Ranger (version 6.0.0) was used for barcode processing, unique molecular identifiers filtering, gene counting, and sample mapping to the reference transcriptome (GRCh38). The filtered UMI count matrix was provided from Cell Ranger as an input in the Seurat workflow (version 4.0).(40) Nuclei with less than 200 and greater than 6,000 (for the male sample) or 8,000 (for the female sample) detected genes based on read depth were filtered out to eliminate low quality nuclei and multiplets. Nuclei with more than 5% mitochondrial genes detected were further removed. After filtering, a total of 6,591 nuclei were obtained, 2,782 nuclei for the male sample and 3,809 nuclei for the female sample.

We applied the anchor-based strategy in the Seurat workflow to integrate samples from different batches. To merge two samples, both male and female count matrices were log-normalized in Seurat's function 'NormalizeData' and the top 2,000 shared highly variable genes were found using the function 'FinderVariableFeatures' with "selection.method = 'vst'". The integration anchors were then identified using the canonical correlation analysis from the function 'FinderIntegrationAnchors'. Based on the anchors, two datasets were integrated using the function 'IntegrateData'.

Principal component analysis (PCA) was performed on the integrated dataset. Based on the first 30 principal components (PC), the uniform manifold approximation and projection (UMAP) was used for dimension reduction. A shared nearest neighbor (SNN) graph was built with the first 30 PCs using Seurat's function 'FindNeighbors'. The nuclei were clustered using a Louvain algorithm applied by the function 'FindClusters'.

Identification of microglia nuclei

887 Cell types were annotated based on the reference dataset(38) using Seurat's label-
888 transferring approach. The identified nuclei clusters were comparable to the unsupervised
889 clustering results under the resolution parameter 0.04. We compared the clusters from
890 reference-based annotation and unsupervised clustering analysis to determine the subset
891 of microglia-specific nuclei.
892 We found a sub-cluster of the reference-annotated microglia (cluster 4 from the
893 unsupervised clustering results) highly expressed T cell signature genes (*THEMIS*,
894 *SKAP1*) (data not shown). These nuclei were excluded in further analysis. The final
895 microglia nuclei were selected as the intersection of the reference-annotated microglia
896 cells and the nuclei from clusters 1 and 3 in unsupervised clustering analysis (boxed in
897 Figure 6c). It was confirmed that microglia marker genes (*ITGAM*, *CTSS*, *CSF1R*, *C1QA*)
898 were highly expressed in these clusters (boxed in Figure 6c and 6d). Using these criteria,
899 2,316 nuclei were classified as microglia and isolated for further analysis.
900
901 **Sub-cluster annotation for microglia nuclei**
902 Using the isolated microglia nuclei, we applied the unsupervised clustering
903 analysis under a series of resolution parameters to investigate biological meaningful
904 subclusters. Microglia were clustered using resolution 0.06 to form 4 clusters. Based on
905 differential gene expression patterns, cluster 0 was further sub-clustered into three
906 additional clusters (cluster 2, 3 and 6). After this regrouping, we ended with 6 total
907 microglia nuclei subclusters (Figure 6e). Differential expression analysis was performed
908 from the function 'FindAllMarkers' in the Seurat package with filtering parameters
909 'min.pct = 0.25' and 'logfc.threshold = 0.25'.
910
911 **Study Approval**
912 All procedures were approved by the Stanford University Administrative Panel on
913 Laboratory Animal Care and the Veterans Affairs Palo Alto Health Care System
914 Institutional Animal Care and Use Committee in accordance with American Veterinary
915 Medical Association guidelines and the International Association for the Study of Pain.
916 Human post-mortem spinal cord was obtained in collaboration with Donor Network West
917 and received Institutional Review Board exemption.
918
919
920

921 **References:**

922 1. Institute of Medicine, "Relieving Pain in America: A Blueprint for Transforming
923 Prevention, Care, Education, and Research" (2011).

924 2. L. J. Zhou, J. Peng, Y. N. Xu, W. J. Zeng, J. Zhang, X. Wei, C. L. Mai, Z. J. Lin, Y. Liu,
925 M. Murugan, U. B. Eyo, A. D. Umpierre, W. J. Xin, T. Chen, M. Li, H. Wang, J. R.
926 Richardson, Z. Tan, X. G. Liu, L. J. Wu, Microglia Are Indispensable for Synaptic
927 Plasticity in the Spinal Dorsal Horn and Chronic Pain. *Cell reports* **27**, 3844-3859 e3846
928 (2019).

929 3. E. S. Haight, T. E. Forman, S. A. Cordonnier, M. L. James, V. L. Tawfik, Microglial
930 Modulation as a Target for Chronic Pain: From the Bench to the Bedside and Back.
931 *Anesthesia and analgesia* **128**, 737-746 (2019).

932 4. R. R. Ji, A. Chamessian, Y. Q. Zhang, Pain regulation by non-neuronal cells and
933 inflammation. *Science* **354**, 572-577 (2016).

934 5. M. H. Yi, Y. U. Liu, K. Liu, T. Chen, D. B. Bosco, J. Zheng, M. Xie, L. Zhou, W. Qu, L.
935 J. Wu, Chemogenetic manipulation of microglia inhibits neuroinflammation and
936 neuropathic pain in mice. *Brain, behavior, and immunity* **92**, 78-89 (2021).

937 6. V. L. Tawfik, N. Nutile-McMenemy, M. L. Lacroix-Fralish, J. A. Deleo, Efficacy of
938 propentofylline, a glial modulating agent, on existing mechanical allodynia following
939 peripheral nerve injury. *Brain, behavior, and immunity* **21**, 238-246 (2007).

940 7. R. R. Ji, T. Berta, M. Nedergaard, Glia and pain: is chronic pain a gliopathy? *Pain* **154**
941 **Suppl 1**, S10-28 (2013).

942 8. N. A. Huck, J. Siliezar-Doyle, E. S. Haight, R. Ishida, T. E. Forman, S. Wu, H. Shen, Y.
943 Takemura, J. D. Clark, V. L. Tawfik, Temporal Contribution of Myeloid-Lineage TLR4
944 to the Transition to Chronic Pain: A Focus on Sex Differences. *The Journal of*
945 *neuroscience : the official journal of the Society for Neuroscience* **41**, 4349-4365 (2021).

946 9. N. Gu, J. Peng, M. Murugan, X. Wang, U. B. Eyo, D. Sun, Y. Ren, E. DiCicco-Bloom,
947 W. Young, H. Dong, L. J. Wu, Spinal Microgliosis Due to Resident Microglial
948 Proliferation Is Required for Pain Hypersensitivity after Peripheral Nerve Injury. *Cell*
949 *reports* **16**, 605-614 (2016).

950 10. S. Echeverry, X. Q. Shi, M. Yang, H. Huang, Y. Wu, L. E. Lorenzo, J. Perez-Sanchez, R.
951 P. Bonin, Y. De Koninck, J. Zhang, Spinal microglia are required for long-term
952 maintenance of neuropathic pain. *Pain* **158**, 1792-1801 (2017).

953 11. R. E. Sorge, J. C. Mapplebeck, S. Rosen, S. Beggs, S. Taves, J. K. Alexander, L. J.
954 Martin, J. S. Austin, S. G. Sotocinal, D. Chen, M. Yang, X. Q. Shi, H. Huang, N. J.
955 Pillon, P. J. Bilan, Y. Tu, A. Klip, R. R. Ji, J. Zhang, M. W. Salter, J. S. Mogil, Different
956 immune cells mediate mechanical pain hypersensitivity in male and female mice. *Nature*
957 *neuroscience* **18**, 1081-1083 (2015).

958 12. J. Peng, N. Gu, L. Zhou, B. E. U, M. Murugan, W. B. Gan, L. J. Wu, Microglia and
959 monocytes synergistically promote the transition from acute to chronic pain after nerve
960 injury. *Nature communications* **7**, 12029 (2016).

961 13. C. N. Parkhurst, G. Yang, I. Ninan, J. N. Savas, J. R. Yates, 3rd, J. J. Lafaille, B. L.
962 Hempstead, D. R. Littman, W. B. Gan, Microglia promote learning-dependent synapse
963 formation through brain-derived neurotrophic factor. *Cell* **155**, 1596-1609 (2013).

964 14. Y. Lavin, D. Winter, R. Blecher-Gonen, E. David, H. Keren-Shaul, M. Merad, S. Jung, I.
965 Amit, Tissue-resident macrophage enhancer landscapes are shaped by the local
966 microenvironment. *Cell* **159**, 1312-1326 (2014).

967 15. D. Gosselin, V. M. Link, C. E. Romanoski, G. J. Fonseca, D. Z. Eichenfield, N. J. Spann,
968 J. D. Stender, H. B. Chun, H. Garner, F. Geissmann, C. K. Glass, Environment drives
969 selection and function of enhancers controlling tissue-specific macrophage identities. *Cell*
970 **159**, 1327-1340 (2014).

971 16. L. M. De Biase, A. Bonci, Region-Specific Phenotypes of Microglia: The Role of Local
972 Regulatory Cues. *The Neuroscientist : a review journal bringing neurobiology, neurology*
973 *and psychiatry* **25**, 314-333 (2019).

974 17. L. M. De Biase, K. E. Schuebel, Z. H. Fusfeld, K. Jair, I. A. Hawes, R. Cimbro, H. Y.
975 Zhang, Q. R. Liu, H. Shen, Z. X. Xi, D. Goldman, A. Bonci, Local Cues Establish and
976 Maintain Region-Specific Phenotypes of Basal Ganglia Microglia. *Neuron* **95**, 341-356
977 e346 (2017).

978 18. K. Grabert, T. Michoel, M. H. Karavolos, S. Clohisey, J. K. Baillie, M. P. Stevens, T. C.
979 Freeman, K. M. Summers, B. W. McColl, Microglial brain region-dependent diversity
980 and selective regional sensitivities to aging. *Nature neuroscience* **19**, 504-516 (2016).

981 19. O. Butovsky, M. P. Jedrychowski, C. S. Moore, R. Cialic, A. J. Lanser, G. Gabriely, T.
982 Koeglsperger, B. Dake, P. M. Wu, C. E. Doykan, Z. Fanek, L. Liu, Z. Chen, J. D.
983 Rothstein, R. M. Ransohoff, S. P. Gygi, J. P. Antel, H. L. Weiner, Identification of a
984 unique TGF-beta-dependent molecular and functional signature in microglia. *Nature*
985 *neuroscience* **17**, 131-143 (2014).

986 20. T. Fernandez-Zafra, T. Gao, A. Jurczak, K. Sandor, Z. Hore, N. M. Agalave, J. Su, J.
987 Estelius, J. Lampa, T. Hokfelt, Z. Wiesenfeld-Hallin, X. Xu, F. Denk, C. I. Svensson,
988 Exploring the transcriptome of resident spinal microglia after collagen antibody-induced
989 arthritis. *Pain* **160**, 224-236 (2019).

990 21. S. Tansley, S. Uttam, A. Urena Guzman, M. Yaqubi, A. Pacis, M. Parisien, H. Deamond,
991 C. Wong, O. Rabau, N. Brown, L. Haglund, J. Ouellet, C. Santaguida, A. Ribeiro-da-
992 Silva, S. Tahmasebi, M. Prager-Khoutorsky, J. Ragoussis, J. Zhang, M. W. Salter, L.
993 Diatchenko, L. M. Healy, J. S. Mogil, A. Khoutorsky, Single-cell RNA sequencing
994 reveals time- and sex-specific responses of mouse spinal cord microglia to peripheral
995 nerve injury and links ApoE to chronic pain. *Nature communications* **13**, 843 (2022).

996 22. D. Gosselin, D. Skola, N. G. Coufal, I. R. Holtman, J. C. M. Schlachetzki, E. Sajti, B. N.
997 Jaeger, C. O'Connor, C. Fitzpatrick, M. P. Pasillas, M. Pena, A. Adair, D. D. Gonda, M.
998 L. Levy, R. M. Ransohoff, F. H. Gage, C. K. Glass, An environment-dependent
999 transcriptional network specifies human microglia identity. *Science* **356**, (2017).

1000 23. T. Masuda, R. Sankowski, O. Staszewski, C. Bottcher, L. Amann, Sagar, C. Scheiwe, S.
1001 Nessler, P. Kunz, G. van Loo, V. A. Coenen, P. C. Reinacher, A. Michel, U. Sure, R.
1002 Gold, D. Grun, J. Priller, C. Stadelmann, M. Prinz, Spatial and temporal heterogeneity of
1003 mouse and human microglia at single-cell resolution. *Nature* **566**, 388-392 (2019).

1004 24. J. Bruttger, K. Karram, S. Wortge, T. Regen, F. Marini, N. Hoppmann, M. Klein, T.
1005 Blank, S. Yona, Y. Wolf, M. Mack, E. Pinteaux, W. Muller, F. Zipp, H. Binder, T. Bopp,
1006 M. Prinz, S. Jung, A. Waisman, Genetic Cell Ablation Reveals Clusters of Local Self-
1007 Renewing Microglia in the Mammalian Central Nervous System. *Immunity* **43**, 92-106
1008 (2015).

1009 25. H. C. Cropper, E. M. Johnson, E. S. Haight, S. A. Cordonnier, A. M. Chaney, T. E.
1010 Forman, A. Biswal, M. Y. Stevens, M. L. James, V. L. Tawfik, Longitudinal translocator
1011 protein-18 kDa-positron emission tomography imaging of peripheral and central myeloid
1012 cells in a mouse model of complex regional pain syndrome. *Pain* **160**, 2136-2148 (2019).

1013 26. T. S. Heng, M. W. Painter, C. Immunological Genome Project, The Immunological
1014 Genome Project: networks of gene expression in immune cells. *Nature immunology* **9**,
1015 1091-1094 (2008).

1016 27. F. Denk, M. Crow, A. Didangelos, D. M. Lopes, S. B. McMahon, Persistent Alterations
1017 in Microglial Enhancers in a Model of Chronic Pain. *Cell reports* **15**, 1771-1781 (2016).

1018 28. L. E. Pena-Altamira, E. Polazzi, P. Giuliani, A. Beraudi, F. Massenzio, I. Mengoni, A.
1019 Poli, M. Zuccarini, R. Ciccarelli, P. Di Iorio, M. Virgili, B. Monti, F. Caciagli, Release of
1020 soluble and vesicular purine nucleoside phosphorylase from rat astrocytes and microglia
1021 induced by pro-inflammatory stimulation with extracellular ATP via P2X(7) receptors.
1022 *Neurochemistry international* **115**, 37-49 (2018).

1023 29. S. M. Jung, L. Peyton, H. Essa, D. S. Choi, Adenosine receptors: Emerging non-opioids
1024 targets for pain medications. *Neurobiol Pain* **11**, 100087 (2022).

1025 30. A. Kumanogoh, C. Watanabe, I. Lee, X. Wang, W. Shi, H. Araki, H. Hirata, K. Iwahori,
1026 J. Uchida, T. Yasui, M. Matsumoto, K. Yoshida, H. Yakura, C. Pan, J. R. Parnes, H.
1027 Kikutani, Identification of CD72 as a lymphocyte receptor for the class IV semaphorin
1028 CD100: a novel mechanism for regulating B cell signaling. *Immunity* **13**, 621-631 (2000).

1029 31. T. Okuno, Y. Nakatsuji, M. Moriya, H. Takamatsu, S. Nojima, N. Takegahara, T.
1030 Toyofuku, Y. Nakagawa, S. Kang, R. H. Friedel, S. Sakoda, H. Kikutani, A. Kumanogoh,
1031 Roles of Sema4D-plexin-B1 interactions in the central nervous system for pathogenesis
1032 of experimental autoimmune encephalomyelitis. *Journal of immunology* **184**, 1499-1506
1033 (2010).

1034 32. R. R. Ji, Z. Z. Xu, Y. J. Gao, Emerging targets in neuroinflammation-driven chronic pain.
1035 *Nature reviews. Drug discovery* **13**, 533-548 (2014).

1036 33. Z. C. Lv, X. Y. Cao, Y. X. Guo, X. D. Zhang, J. Ding, J. Geng, K. Feng, H. Niu, MiR-
1037 137-5p alleviates inflammation by upregulating IL-10R1 expression in rats with spinal
1038 cord injury. *Eur Rev Med Pharmacol Sci* **23**, 4551-4557 (2019).

1039 34. F. Borrego, The CD300 molecules: an emerging family of regulators of the immune
1040 system. *Blood* **121**, 1951-1960 (2013).

1041 35. D. E. Clapham, Calcium signaling. *Cell* **131**, 1047-1058 (2007).

1042 36. K. Montague-Cardoso, M. Malcangio, Cathepsin S as a potential therapeutic target for
1043 chronic pain. *Med Drug Discov* **7**, 100047 (2020).

1044 37. Y. Hayashi, S. Koyanagi, N. Kusunose, R. Okada, Z. Wu, H. Tozaki-Saitoh, K. Ukai, S.
1045 Kohsaka, K. Inoue, S. Ohdo, H. Nakanishi, The intrinsic microglial molecular clock
1046 controls synaptic strength via the circadian expression of cathepsin S. *Scientific reports* **3**,
1047 2744 (2013).

1048 38. N. Habib, I. Avraham-Davidi, A. Basu, T. Burks, K. Shekhar, M. Hofree, S. R.
1049 Choudhury, F. Aguet, E. Gelfand, K. Ardlie, D. A. Weitz, O. Rozenblatt-Rosen, F.
1050 Zhang, A. Regev, Massively parallel single-nucleus RNA-seq with DroNc-seq. *Nature*
1051 *methods* **14**, 955-958 (2017).

1052 39. K. J. E. Matson, D. E. Russ, C. Kathe, I. Hua, D. Maric, Y. Ding, J. Krynitsky, R.
1053 Pursley, A. Sathyamurthy, J. W. Squair, B. P. Levi, G. Courtine, A. J. Levine, Single cell
1054 atlas of spinal cord injury in mice reveals a pro-regenerative signature in spinocerebellar
1055 neurons. *Nature communications* **13**, 5628 (2022).

1056 40. T. Stuart, A. Butler, P. Hoffman, C. Hafemeister, E. Papalexi, W. M. Mauck, 3rd, Y.
1057 Hao, M. Stoeckius, P. Smibert, R. Satija, Comprehensive Integration of Single-Cell Data.
1058 *Cell* **177**, 1888-1902 e1821 (2019).

1059 41. H. Yang, L. Wu, H. Deng, Y. Chen, H. Zhou, M. Liu, S. Wang, L. Zheng, L. Zhu, X. Lv,
1060 Anti-inflammatory protein TSG-6 secreted by bone marrow mesenchymal stem cells
1061 attenuates neuropathic pain by inhibiting the TLR2/MyD88/NF-kappaB signaling
1062 pathway in spinal microglia. *Journal of neuroinflammation* **17**, 154 (2020).

1063 42. D. S. A. Simpson, P. L. Oliver, ROS Generation in Microglia: Understanding Oxidative
1064 Stress and Inflammation in Neurodegenerative Disease. *Antioxidants (Basel)* **9**, (2020).

1065 43. M. Baek, J. C. Chai, H. I. Choi, E. Yoo, B. Binas, Y. S. Lee, K. H. Jung, Y. G. Chai.
1066 (Research Square, 2022).

1067 44. M. Neidlin, S. Dimitrakopoulou, L. G. Alexopoulos, Multi-tissue network analysis for
1068 drug prioritization in knee osteoarthritis. *Scientific reports* **9**, 15176 (2019).

1069 45. D. G. Topouza, J. Choi, S. Nesdoly, A. Tarnouskaya, C. J. B. Nicol, Q. L. Duan, Novel
1070 MicroRNA-Regulated Transcript Networks Are Associated with Chemotherapy
1071 Response in Ovarian Cancer. *International journal of molecular sciences* **23**, (2022).

1072 46. Y. Chen, M. Colonna, Microglia in Alzheimer's disease at single-cell level. Are there
1073 common patterns in humans and mice? *The Journal of experimental medicine* **218**,
1074 (2021).

1075 47. M. H. Yi, Y. U. Liu, A. D. Umpierre, T. Chen, Y. Ying, J. Zheng, A. Dheer, D. B. Bosco,
1076 H. Dong, L. J. Wu, Optogenetic activation of spinal microglia triggers chronic pain in
1077 mice. *PLoS Biol* **19**, e3001154 (2021).

1078 48. F. R. Nieto, A. K. Clark, J. Grist, V. Chapman, M. Malcangio, Calcitonin gene-related
1079 peptide-expressing sensory neurons and spinal microglial reactivity contribute to pain
1080 states in collagen-induced arthritis. *Arthritis Rheumatol* **67**, 1668-1677 (2015).

1081 49. M. Mousseau, N. E. Burma, K. Y. Lee, H. Leduc-Pessah, C. H. T. Kwok, A. R. Reid, M.
1082 O'Brien, B. Sagalajev, J. A. Stratton, N. Patrick, P. L. Stemkowski, J. Biernaskie, G. W.
1083 Zamponi, P. Salo, J. J. McDougall, S. A. Prescott, J. R. Matyas, T. Trang, Microglial
1084 pannexin-1 channel activation is a spinal determinant of joint pain. *Science advances* **4**,
1085 eaas9846 (2018).

1086 50. K. Kohno, R. Shirasaka, K. Yoshihara, S. Mikuriya, K. Tanaka, K. Takanami, K. Inoue,
1087 H. Sakamoto, Y. Ohkawa, T. Masuda, M. Tsuda, A spinal microglia population involved
1088 in remitting and relapsing neuropathic pain. *Science* **376**, 86-90 (2022).

1089 51. R. E. Sorge, M. L. LaCroix-Fralish, A. H. Tuttle, S. G. Sotocinal, J. S. Austin, J. Ritchie,
1090 M. L. Chanda, A. C. Graham, L. Topham, S. Beggs, M. W. Salter, J. S. Mogil, Spinal
1091 cord Toll-like receptor 4 mediates inflammatory and neuropathic hypersensitivity in male
1092 but not female mice. *The Journal of neuroscience : the official journal of the Society for*
1093 *Neuroscience* **31**, 15450-15454 (2011).

1094 52. S. Lee, X. Q. Shi, A. Fan, B. West, J. Zhang, Targeting macrophage and microglia
1095 activation with colony stimulating factor 1 receptor inhibitor is an effective strategy to
1096 treat injury-triggered neuropathic pain. *Mol Pain* **14**, 1744806918764979 (2018).

1097 53. I. Decosterd, C. J. Woolf, Spared nerve injury: an animal model of persistent peripheral
1098 neuropathic pain. *Pain* **87**, 149-158 (2000).

1099 54. S. H. Kim, J. M. Chung, An experimental model for peripheral neuropathy produced by
1100 segmental spinal nerve ligation in the rat. *Pain* **50**, 355-363 (1992).

1101 55. E. S. Haight, E. M. Johnson, I. R. Carroll, V. L. Tawfik, Of mice, microglia, and
1102 (wo)men: a case series and mechanistic investigation of hydroxychloroquine for complex
1103 regional pain syndrome. *Pain reports* **5**, e841 (2020).

1104 56. B. Basilico, L. Ferrucci, P. Ratano, M. T. Golia, A. Grimaldi, M. Rosito, V. Ferretti, I.
1105 Reverte, C. Sanchini, M. C. Marrone, M. Giubettini, V. De Turris, D. Salerno, S.

1106 Garofalo, M. K. St-Pierre, M. Carrier, M. Renzi, F. Pagani, B. Modi, M. Raspa, F.
1107 Scavizzi, C. T. Gross, S. Marinelli, M. E. Tremblay, D. Caprioli, L. Maggi, C. Limatola,
1108 S. Di Angelantonio, D. Ragozzino, Microglia control glutamatergic synapses in the adult
1109 mouse hippocampus. *Glia* **70**, 173-195 (2022).

1110 57. R. A. Rice, J. Pham, R. J. Lee, A. R. Najafi, B. L. West, K. N. Green, Microglial
1111 repopulation resolves inflammation and promotes brain recovery after injury. *Glia* **65**,
1112 931-944 (2017).

1113 58. Y. Yao, S. Echeverry, X. Q. Shi, M. Yang, Q. Z. Yang, G. Y. Wang, J. Chambon, Y. C.
1114 Wu, K. Y. Fu, Y. De Koninck, J. Zhang, Dynamics of spinal microglia repopulation
1115 following an acute depletion. *Scientific reports* **6**, 22839 (2016).

1116 59. Y. Huang, Z. Xu, S. Xiong, F. Sun, G. Qin, G. Hu, J. Wang, L. Zhao, Y. X. Liang, T.
1117 Wu, Z. Lu, M. S. Humayun, K. F. So, Y. Pan, N. Li, T. F. Yuan, Y. Rao, B. Peng,
1118 Repopulated microglia are solely derived from the proliferation of residual microglia
1119 after acute depletion. *Nature neuroscience* **21**, 530-540 (2018).

1120 60. R. C. Paolicelli, A. Sierra, B. Stevens, M. E. Tremblay, A. Aguzzi, B. Ajami, I. Amit, E.
1121 Audinat, I. Bechmann, M. Bennett, F. Bennett, A. Bessis, K. Biber, S. Bilbo, M. Blurton-
1122 Jones, E. Boddeke, D. Brites, B. Brone, G. C. Brown, O. Butovsky, M. J. Carson, B.
1123 Castellano, M. Colonna, S. A. Cowley, C. Cunningham, D. Davalos, P. L. De Jager, B.
1124 de Strooper, A. Denes, B. J. L. Eggen, U. Eyo, E. Galea, S. Garel, F. Ginhoux, C. K.
1125 Glass, O. Gokce, D. Gomez-Nicola, B. Gonzalez, S. Gordon, M. B. Graeber, A. D.
1126 Greenhalgh, P. Gressens, M. Greter, D. H. Gutmann, C. Haass, M. T. Heneka, F. L.
1127 Heppner, S. Hong, D. A. Hume, S. Jung, H. Kettenmann, J. Kipnis, R. Koyama, G.
1128 Lemke, M. Lynch, A. Majewska, M. Malcangio, T. Malm, R. Mancuso, T. Masuda, M.
1129 Matteoli, B. W. McColl, V. E. Miron, A. V. Molofsky, M. Monje, E. Mracsko, A.
1130 Nadjar, J. J. Neher, U. Neniskyte, H. Neumann, M. Noda, B. Peng, F. Peri, V. H. Perry,
1131 P. G. Popovich, C. Pridans, J. Priller, M. Prinz, D. Ragozzino, R. M. Ransohoff, M. W.
1132 Salter, A. Schaefer, D. P. Schafer, M. Schwartz, M. Simons, C. J. Smith, W. J. Streit, T.
1133 L. Tay, L. H. Tsai, A. Verkhratsky, R. von Bernhardi, H. Wake, V. Wittamer, S. A. Wolf,
1134 L. J. Wu, T. Wyss-Coray, Microglia states and nomenclature: A field at its crossroads.
1135 *Neuron* **110**, 3458-3483 (2022).

1136 61. T. R. Hammond, C. Dufort, L. Dissing-Olesen, S. Giera, A. Young, A. Wysoker, A. J.
1137 Walker, F. Gergits, M. Segel, J. Nemesh, S. E. Marsh, A. Saunders, E. Macosko, F.
1138 Ginhoux, J. Chen, R. J. M. Franklin, X. Piao, S. A. McCarroll, B. Stevens, Single-Cell
1139 RNA Sequencing of Microglia throughout the Mouse Lifespan and in the Injured Brain
1140 Reveals Complex Cell-State Changes. *Immunity* **50**, 253-271.e256 (2019).

1141 62. H. Keren-Shaul, A. Spinrad, A. Weiner, O. Matcovitch-Natan, R. Dvir-Szternfeld, T. K.
1142 Ulland, E. David, K. Baruch, D. Lara-Astaiso, B. Toth, S. Itzkovitz, M. Colonna, M.
1143 Schwartz, I. Amit, A Unique Microglia Type Associated with Restricting Development
1144 of Alzheimer's Disease. *Cell* **169**, 1276-1290 e1217 (2017).

1145 63. M. Absinta, D. Maric, M. Gharagozloo, T. Garton, M. D. Smith, J. Jin, K. C. Fitzgerald,
1146 A. Song, P. Liu, J. P. Lin, T. Wu, K. R. Johnson, D. B. McGavern, D. P. Schafer, P. A.
1147 Calabresi, D. S. Reich, A lymphocyte-microglia-astrocyte axis in chronic active multiple
1148 sclerosis. *Nature* **597**, 709-714 (2021).

1149 64. A. Yadav, K. J. E. Matson, L. Li, I. Hua, J. Petrescu, K. Kang, M. R. Alkaslasi, D. I. Lee,
1150 S. Hasan, A. Galuta, A. Dedek, S. Ameri, J. Parnell, M. M. Alshardan, F. A. Qumqumji,
1151 S. M. Alhamad, A. P. Wang, G. Poulen, N. Lonjon, F. Vachiery-Lahaye, P. Gaur, M. A.
1152 Nalls, Y. A. Qi, M. E. Ward, M. E. Hildebrand, P.-F. Mery, E. Bourinet, L. Bauchet, E.
1153 C. Tsai, H. Phatnani, C. E. Le Pichon, V. Menon, A. J. Levine, A Cellular Taxonomy of
1154 the Adult Human Spinal Cord. *bioRxiv*, 2022.2003.2025.485808 (2022).

1155 65. T. Yvanka de Soysa, M. Therrien, A. C. Walker, B. Stevens, Redefining microglia states:
1156 Lessons and limits of human and mouse models to study microglia states in
1157 neurodegenerative diseases. *Semin Immunol* **60**, 101651 (2022).

1158 66. F. L. Xuan, K. Chithanathan, K. Lillevali, X. Yuan, L. Tian, Differences of Microglia in
1159 the Brain and the Spinal Cord. *Frontiers in cellular neuroscience* **13**, 504 (2019).

1160 67. L. Geirsdottir, E. David, H. Keren-Shaul, A. Weiner, S. C. Bohlen, J. Neuber, A. Balic,
1161 A. Giladi, F. Sheban, C. A. Dutertre, C. Pfeifle, F. Peri, A. Raffo-Romero, J. Vizioli, K.
1162 Matiasek, C. Scheiwe, S. Meckel, K. Matz-Rensing, F. van der Meer, F. R.
1163 Thormodsson, C. Stadelmann, N. Zilkha, T. Kimchi, F. Ginhoux, I. Ulitsky, D. Erny, I.
1164 Amit, M. Prinz, Cross-Species Single-Cell Analysis Reveals Divergence of the Primate
1165 Microglia Program. *Cell* **179**, 1609-1622 e1616 (2019).

1166 68. G. J. Clark, X. Ju, C. Tate, D. N. Hart, The CD300 family of molecules are evolutionarily
1167 significant regulators of leukocyte functions. *Trends in immunology* **30**, 209-217 (2009).

1168 69. E. J. Kim, S. M. Lee, K. Suk, W. H. Lee, CD300a and CD300f differentially regulate the
1169 MyD88 and TRIF-mediated TLR signalling pathways through activation of SHP-1 and/or
1170 SHP-2 in human monocytic cell lines. *Immunology* **135**, 226-235 (2012).

1171 70. H. Peluffo, D. Ali-Ruiz, A. Ejarque-Ortiz, V. Heras-Alvarez, E. Comas-Casellas, A.
1172 Martinez-Barriocanal, A. Kamaid, D. Alvarez-Errico, M. L. Negro, N. Lago, S.
1173 Schwartz, Jr., A. Villaverde, J. Sayos, Overexpression of the immunoreceptor CD300f
1174 has a neuroprotective role in a model of acute brain injury. *Brain Pathol* **22**, 318-328
1175 (2012).

1176 71. T. Keswani, J. Roland, F. Herbert, D. Delcroix-Genete, H. Bauderlique-Le Roy, L.
1177 Gaayeb, P. A. Cazenave, S. Pied, Expression of CD300lf by microglia contributes to
1178 resistance to cerebral malaria by impeding the neuroinflammation. *Genes and immunity*
1179 **21**, 45-62 (2020).

1180 72. Y. C. Hsieh, J. Negri, A. He, R. V. Pearse, 2nd, L. Liu, D. M. Duong, L. B. Chibnik, D.
1181 A. Bennett, N. T. Seyfried, T. L. Young-Pearse, Elevated ganglioside GM2 activator
1182 (GM2A) in human brain tissue reduces neurite integrity and spontaneous neuronal
1183 activity. *Molecular neurodegeneration* **17**, 61 (2022).

1184 73. F. Birklein, A. Ibrahim, T. Schlereth, W. S. Kingery, The Rodent Tibia Fracture Model:
1185 A Critical Review and Comparison With the Complex Regional Pain Syndrome
1186 Literature. *The journal of pain : official journal of the American Pain Society* **19**, 1102
1187 e1101-1102 e1119 (2018).

1188 74. T. Z. Guo, T. Wei, W. W. Li, X. Q. Li, J. D. Clark, W. S. Kingery, Immobilization
1189 contributes to exaggerated neuropeptide signaling, inflammatory changes, and
1190 nociceptive sensitization after fracture in rats. *The journal of pain : official journal of the*
1191 *American Pain Society* **15**, 1033-1045 (2014).

1192 75. R. E. Sorge, L. J. Martin, K. A. Isbester, S. G. Sotocinal, S. Rosen, A. H. Tuttle, J. S.
1193 Wieskopf, E. L. Acland, A. Dokova, B. Kadoura, P. Leger, J. C. Mapplebeck, M.
1194 McPhail, A. Delaney, G. Wigerblad, A. P. Schumann, T. Quinn, J. Frasnelli, C. I.
1195 Svensson, W. F. Sternberg, J. S. Mogil, Olfactory exposure to males, including men,
1196 causes stress and related analgesia in rodents. *Nature methods* **11**, 629-632 (2014).

1197 76. S. R. Chaplan, F. W. Bach, J. W. Pogrel, J. M. Chung, T. L. Yaksh, Quantitative
1198 assessment of tactile allodynia in the rat paw. *Journal of neuroscience methods* **53**, 55-63
1199 (1994).

1200 77. W. W. Li, T. Z. Guo, X. Shi, E. Czirr, T. Stan, P. Sahbaie, T. Wyss-Coray, W. S.
1201 Kingery, J. D. Clark, Autoimmunity contributes to nociceptive sensitization in a mouse
1202 model of complex regional pain syndrome. *Pain* **155**, 2377-2389 (2014).

1203 78. P. A. Ewels, A. Peltzer, S. Fillinger, H. Patel, J. Alneberg, A. Wilm, M. U. Garcia, P. Di
1204 Tommaso, S. Nahnsen, The nf-core framework for community-curated bioinformatics
1205 pipelines. *Nature biotechnology* **38**, 276-278 (2020).

1206 79. P. Di Tommaso, M. Chatzou, E. W. Floden, P. P. Barja, E. Palumbo, C. Notredame,
1207 Nextflow enables reproducible computational workflows. *Nature biotechnology* **35**, 316-
1208 319 (2017).

1209 80. S. Andrews. (2010).

1210 81. F. Krueger, F. James, P. Ewels, E. Afyounian, B. Schuster-Boeckler. (2021).

1211 82. B. Li, C. N. Dewey, RSEM: accurate transcript quantification from RNA-Seq data with
1212 or without a reference genome. *BMC Bioinformatics* **12**, 323 (2011).

1213 83. P. Ewels, M. Magnusson, S. Lundin, M. Kaller, MultiQC: summarize analysis results for
1214 multiple tools and samples in a single report. *Bioinformatics* **32**, 3047-3048 (2016).

1215 84. M. I. Love, W. Huber, S. Anders, Moderated estimation of fold change and dispersion for
1216 RNA-seq data with DESeq2. *Genome Biol* **15**, 550 (2014).

1217 85. P. Langfelder, S. Horvath, WGCNA: an R package for weighted correlation network
1218 analysis. *BMC Bioinformatics* **9**, 559 (2008).

86. U. Raudvere, L. Kolberg, I. Kuzmin, T. Arak, P. Adler, H. Peterson, J. Vilo, g:Profiler: a web server for functional enrichment analysis and conversions of gene lists (2019 update). *Nucleic Acids Res* **47**, W191-W198 (2019).

87. M. Reijnders, R. M. Waterhouse, Summary Visualizations of Gene Ontology Terms With GO-Figure! *Front Bioinform* **1**, 638255 (2021).

88. R. P. Huntley, T. Sawford, P. Mutowo-Meullenet, A. Shypitsyna, C. Bonilla, M. J. Martin, C. O'Donovan, The GOA database: gene Ontology annotation updates for 2015. *Nucleic Acids Res* **43**, D1057-1063 (2015).

89. A. Kramer, J. Green, J. Pollard, Jr., S. Tugendreich, Causal analysis approaches in Ingenuity Pathway Analysis. *Bioinformatics* **30**, 523-530 (2014).

Acknowledgments:

Flow cytometry and Fluorescent Activated Cell Sorting (FACS) was done with instruments in the Palo Alto VA Flow Cytometry Core, which is supported by the US Department of Veterans Affairs (VA), Palo Alto Veterans Institute for Research (PAVIR), and the National Institutes of Health (NIH). Additional cell sorting/flow cytometry analysis for this project was done on instruments in the Stanford Shared FACS Facility. The authors wish to thank Dr. Lianna Bonnano, Dr. Corey Cain, Dr. Alex Lee and Pratima Nallagatla for assistance with FACS and initial bioinformatic analyses. We thank Janelle Siliezar-Doyle and Dylan Mayanja for contributions to initial behavioral analyses. We are also indebted to Dr. Long-Jun Wu and Dr. Min-Hee Yi for training on microglial Sholl analysis. We thank Dr. Brendan Hasz for building the publicly-available website for data sharing and Dr. Arkady Khoutorsky for comments on early versions of this work. This work utilized computing resources and computational and bioinformatics services provided by the Stanford Genetics Bioinformatics Service Center (GBSC).

Funding:

National Institutes of Health (NIH) grant R35GM137906 (VLT)
National Institutes of Health grant T32DA035165 (LJD)
Rita Allen Foundation Scholars Program Fund (VLT)
Philanthropic donation from the Duan Family (VLT)

Author contributions:

Conceptualization: LJD, VLT
Methodology: TF, VLT
Formal analysis: LJD, CMB, ARN, MW, SW, CEJ, ASG, RVN, VLT
Investigation: LJD, ARN, SW, TEF, ESH, NAH, VLT
Writing—original draft: LJD, CMB, ARN, VLT
Writing—review & editing: SW, ESH, NAH, CEJ, ASG, RVN, VLT
Visualization: LJD, CMB, ARN, VLT
Supervision: RVN, VLT
Project administration: VLT
Funding acquisition: LJD, VLT

Competing interests:

Authors declare that they have no competing interests.

Data and materials availability:

Transcriptomic data are included as Extended Data Tables. All transcriptomic data have been deposited as raw FASTQ files in GEO database accession number (in process). We have created two publicly-available, browsable interfaces as a resource for the field https://tawfik-lab-repopulated-microglia-transcrip-streamlit-app-xsbwen.streamlit.app, which includes all transcriptomic bulk-seq mouse spinal cord microglia data and https://tsomics.shinyapps.io/visualization_MGcells/ which includes the human microglial nuclei sequencing data. All other data supporting the findings of this study are available from the corresponding author upon reasonable request.

Figures and Tables:

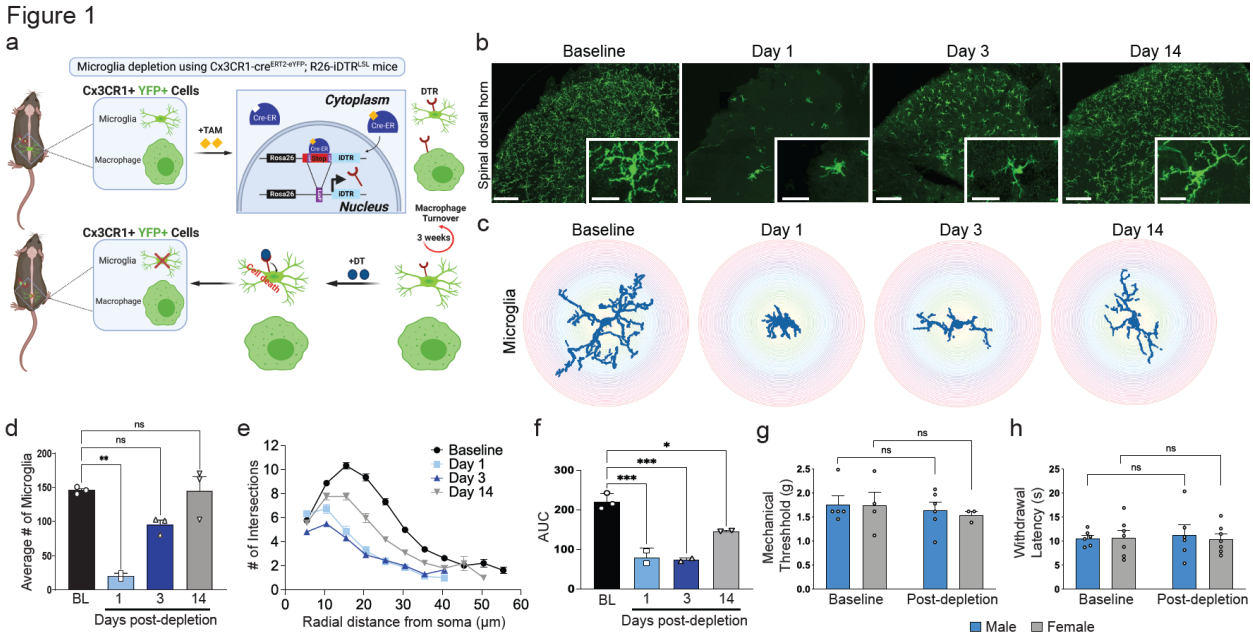

Figure 1. Cx3CR1-cre^{ERT2}-eYFP; R26-iDTR^{LSL} mice exhibit significant loss of microglia after DT-induced depletion but these cells repopulate over time. a) Schematic representation of the strategy used to selectively deplete microglia, and no other myeloid-lineage cells, using the Cx3CR1-cre$^{ERT2-eYFP}$;R26-iDTR^{LSL} mouse. Mice are injected with tamoxifen (TAM, 100 mg/kg daily x 5 days) allowing excision of the floxed STOP codon resulting in all Cx3CR1^{+} cells expressing the DTR. After 21-24 days, high-turnover macrophages no longer express DTR while slow-turnover microglia continue to express DTR. Treatment with diphtheria toxin (DT, 1000 ng daily x 3 days) results in selective death of microglia. b) Lumbar spinal cord sections from Cx3CR1-cre$^{ERT2-eYFP}$; R26-iDTR^{LSL} mice taken at multiple time points before (baseline) or after DT injection demonstrate a significant loss of Iba1^{+} microglia in the dorsal horn at Day 1 post-DT by IHC. Scale bars 100 μm and 20 μm (inset). c) Representative Sholl analysis profiles of microglia demonstrate change in morphology over time following repopulation. d) Quantification of microglia number over time after depletion with DT. Four to five lumbar spinal cord dorsal horn sections were counted and averaged (n= 2-3 mice per group). **$p<0.01$, ****$p<0.0001$ by one-way ANOVA with Tukey's post-hoc test. e) Analysis of intersections at a given radial distance from the soma demonstrates a drop in the number of intersections in repopulating microglia which recovers, though not quite to baseline, over 14 days. f) Area under the curve (AUC) for number of intersections by radial distance from soma demonstrates a time-dependent increase after microglial depletion. *$p<0.05$, ***$p<0.001$ by one-way ANOVA with Dunnett's post-hoc test. Seventy-four to 185 microglia analyzed per time point with n = 2-3 mice per group. g) Microglial-depletion alone does not affect mechanical sensitivity or, h) latency to withdrawal on a 52.5ºC hot plate in male or female Cx3CR1-cre$^{ERT2-eYFP}$;R26-iDTR^{LSL} mice (n = 3-6/sex, comparison by unpaired t-test, in all cases $p>0.05$). ns, not significant. Data are represented as mean ± SEM.

Figure 2

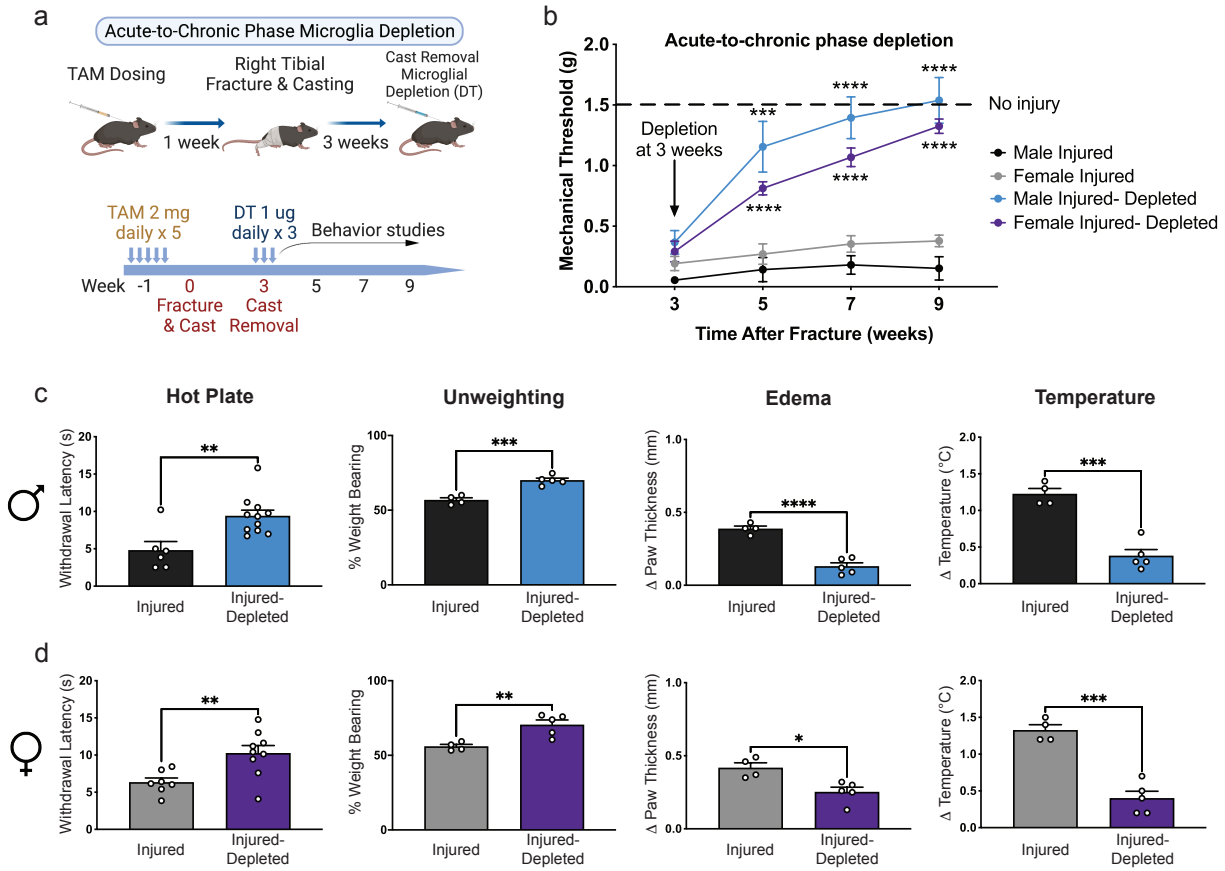

Figure 2. Microglial depletion at the acute-to-chronic phase results in a sustained change in pain trajectory after peripheral injury. a) Schematic of experimental timeline for acute-to-chronic phase depletion of microglia. b) Mechanical threshold is decreased at the time of cast removal (3 weeks) in all groups, however, microglial depletion results in sustained improvement in mechanical sensitivity in both males and females out to 9 weeks post-injury. n = 6-11 per group per sex. ***p<0.001, ****p<0.0001 by two-way ANOVA with Bonferroni's post-hoc test. Microglial depletion at the acute-to-chronic phase additionally results in improvement in thermal sensitivity, weight bearing, edema and temperature changes in both males (c) and females (d) at 4 weeks post-injury. n = 6-11 per group per sex for hot plate, n = 4-5 per group per sex for unweighting, edema and temperature. *p<0.05, **p< 0.01, ***p<0.001 by two-tailed unpaired t-test. Data are represented as mean ± SEM.

Figure 3

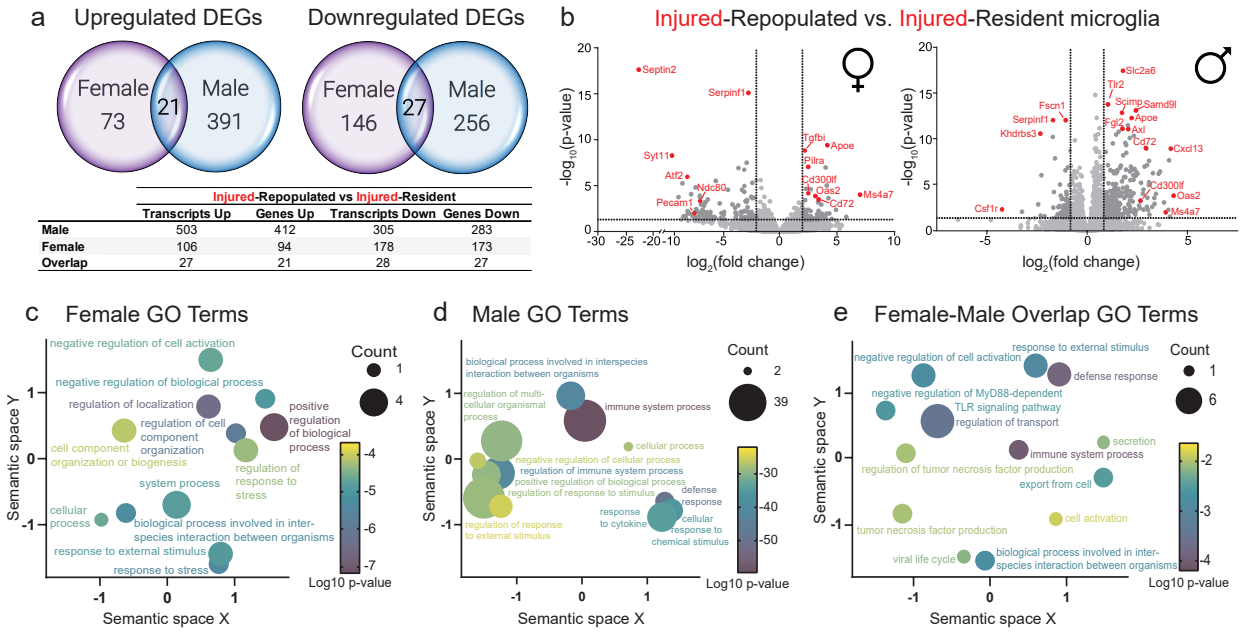

	Injured-Repopulated vs Injured-Resident			
	Transcripts Up	Genes Up	Transcripts Down	Genes Down
Male	503	412	305	283
Female	106	94	178	173
Overlap	27	21	28	27

Figure 3. Differential gene expression analysis of female and male spinal cord microglia after peripheral injury with or without microglia depletion/repopulation identifies sex-specific and sex-independent signatures of pain recovery. a) Differentially expressed microglial transcripts (DETs) and genes (DEGs) were identified using DESeq2 analysis in both males and females. Overall males had more DEGs both up and downregulated compared to females with 21 sex-independent/shared upregulated DEGs and 27 sex-independent/shared downregulated DEGs. b) Volcano plots depicting DEGs from injured-repopulated microglia compared to injured-resident microglia in females (left) and males (right). Highly regulated, sex-independent and significant DEGs are labeled in red. Cutoffs for the x-axis are set at $\log_2$(FC) +/- 2.0 (female) and +/- 0.83 (male). Cutoff for the y-axis is set at p-value = 0.05 for both sexes. Significant gene ontology (GO) terms for females (c) and males (d) based on adjusted p-value > 0.05 for injured-repopulated vs. injured-resident microglia DEGs. e) GO terms for the shared DEGs between male and female injured-repopulated vs. injured-resident microglia. Size of circle represents number of GO terms combined into the parent GO term shown. Color of circle represents log10 p-value.

Figure 4

a Female module-trait relationships

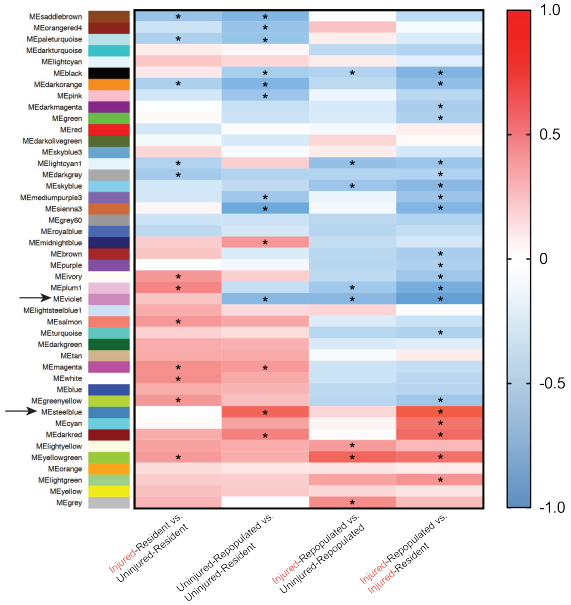

b Male module-trait relationships

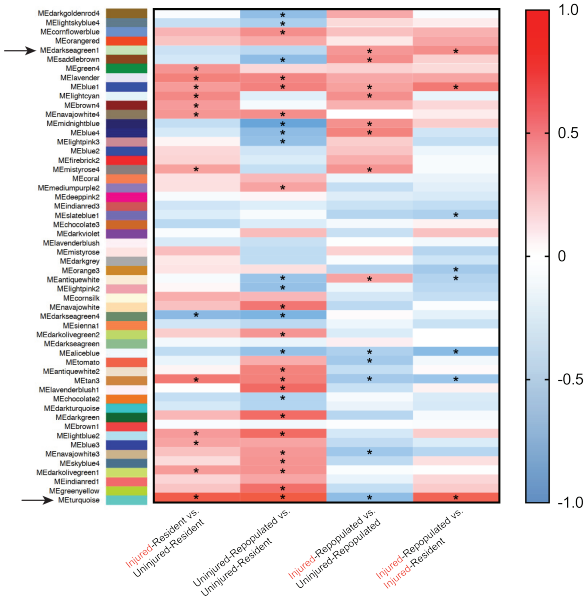

c

Groups Compared	Significant Female Modules	Transcripts in Significant Modules	Significant Male Modules	Transcripts in Significant Modules
Injured-Resident vs Uninjured-Resident	12	2,858	13	9,568
Uninjured-Repop vs Uninjured-Resident	13	3,732	28	15,416
Injured-Repop vs Uninjured-Repop	8	1,705	13	12,513
Injured-Repop vs Injured-Resident	21	15,248	8	11,092
Total Modules	44	26,748	54	28,345

Figure 4. Weighted gene co-expression network analysis (WGCNA) reveals module-trait relationships that are distinct by sex and condition. WGCNA identified 44 unique modules in females (a) and 54 unique modules in males (b) which were then correlated with each of the 4 microglial conditions ("traits"). Module-trait relationships that had significant correlations are marked with an asterisk with heatmaps depicting the strength of the relationship (blue = negative correlation with the first listed group, red = positive correlation with the first listed group). c) The number of significant modules per sex as well as total number of transcripts within each module.

Figure 5

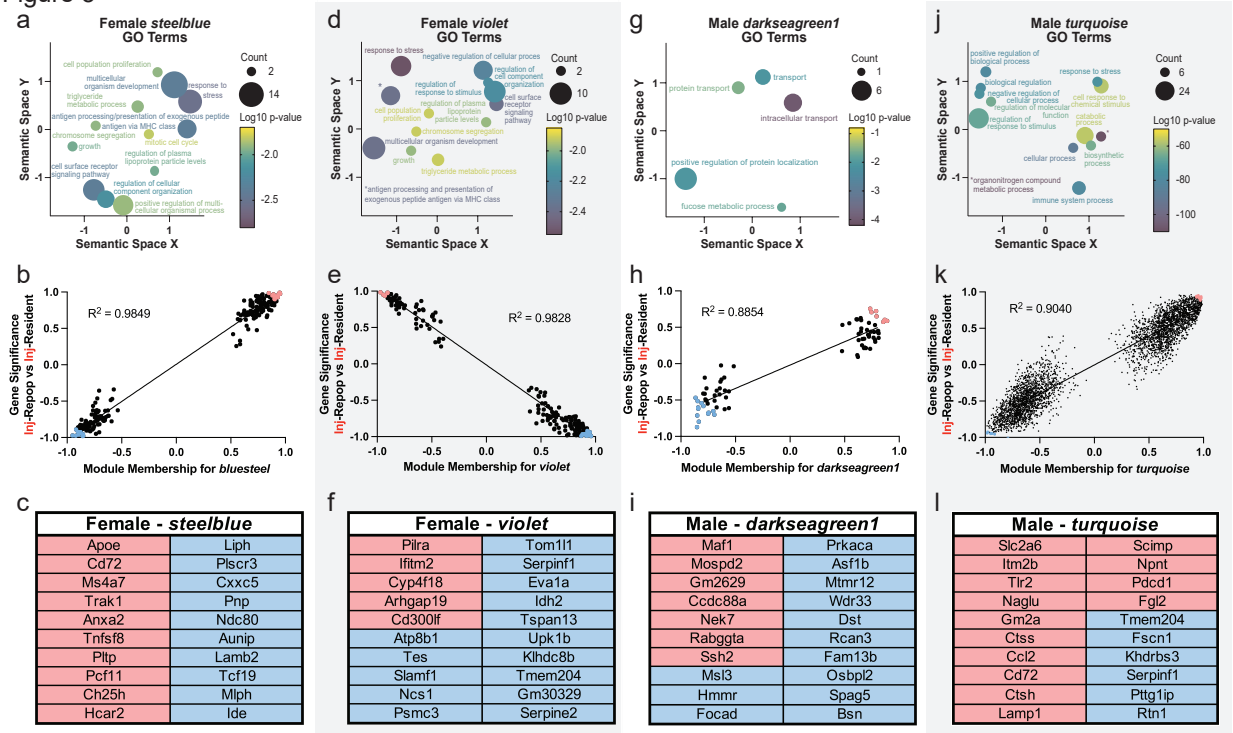

c

Female - *steelblue*	
Apoe	Liph
Cd72	Plscr3
Ms4a7	Cxxc5
Trak1	Pnp
Anxa2	Ndc80
Tnfsf8	Aunip
Pltp	Lamb2
Pcf11	Tcf19
Ch25h	Mlph
Hcar2	Ide

f

Female - *violet*	
Pilra	Tom1l1
Ifitm2	Serpinf1
Cyp4f18	Eva1a
Arhgap19	Idh2
Cd300lf	Tspan13
Atp8b1	Upk1b
Tes	Klhdc8b
Slamf1	Tmem204
Ncs1	Gm30329
Psmc3	Serpine2

i

Male - *darkseagreen1*	
Maf1	Prkaca
Mospd2	Asf1b
Gm2629	Mtmr12
Ccdc88a	Wdr33
Nek7	Dst
Rabggta	Rcan3
Ssh2	Fam13b
Msl3	Osbpl2
Hmmr	Spag5
Focad	Bsn

l

Male - *turquoise*	
Slc2a6	Scimp
Itm2b	Npnt
Tlr2	Pdcd1
Naglu	Fgl2
Gm2a	Tmem204
Ctss	Fscn1
Ccl2	Khdrbs3
Cd72	Serpinf1
Ctsh	Pttg1ip
Lamp1	Rtn1

Figure 5. Modules of interest for each sex highlight networks of genes that may contribute to pain resolution. a) Gene Ontology (GO) terms identified for female module *steelblue*. b) Gene significance vs. module membership plot demonstrates correlation of member genes to the module eigengene. The 20 most extreme genes are highlighted either red for positive fold-change or blue for negative fold-change in the Injured-Repopulated microglia group versus Injured-Resident microglia group. c) List of top 20 most significant genes in gene significance versus module membership correlation for female module *steelblue*. d) GO terms for female module *violet*. e) Gene significance vs. module membership plot for female module *violet*. f) Top 20 most extreme genes for gene significance vs. module membership correlation for female module *violet*. g) GO terms for male module *darkseagreen1*. h) Gene significance vs. module membership for male module *darkseagreen1*. i) Top 20 most extreme genes for gene significance vs. module membership correlation for male module *darkseagreen1*. j) GO terms for male module *turquoise*. k) Gene significance vs. module membership for male module *turquoise*. l) Top 20 most extreme genes for gene significance vs. module membership correlation for male module *turquoise*. Size of circle represents number of GO terms combined into the parent GO term shown. Color of circle represents log10 p-value.

Figure 6

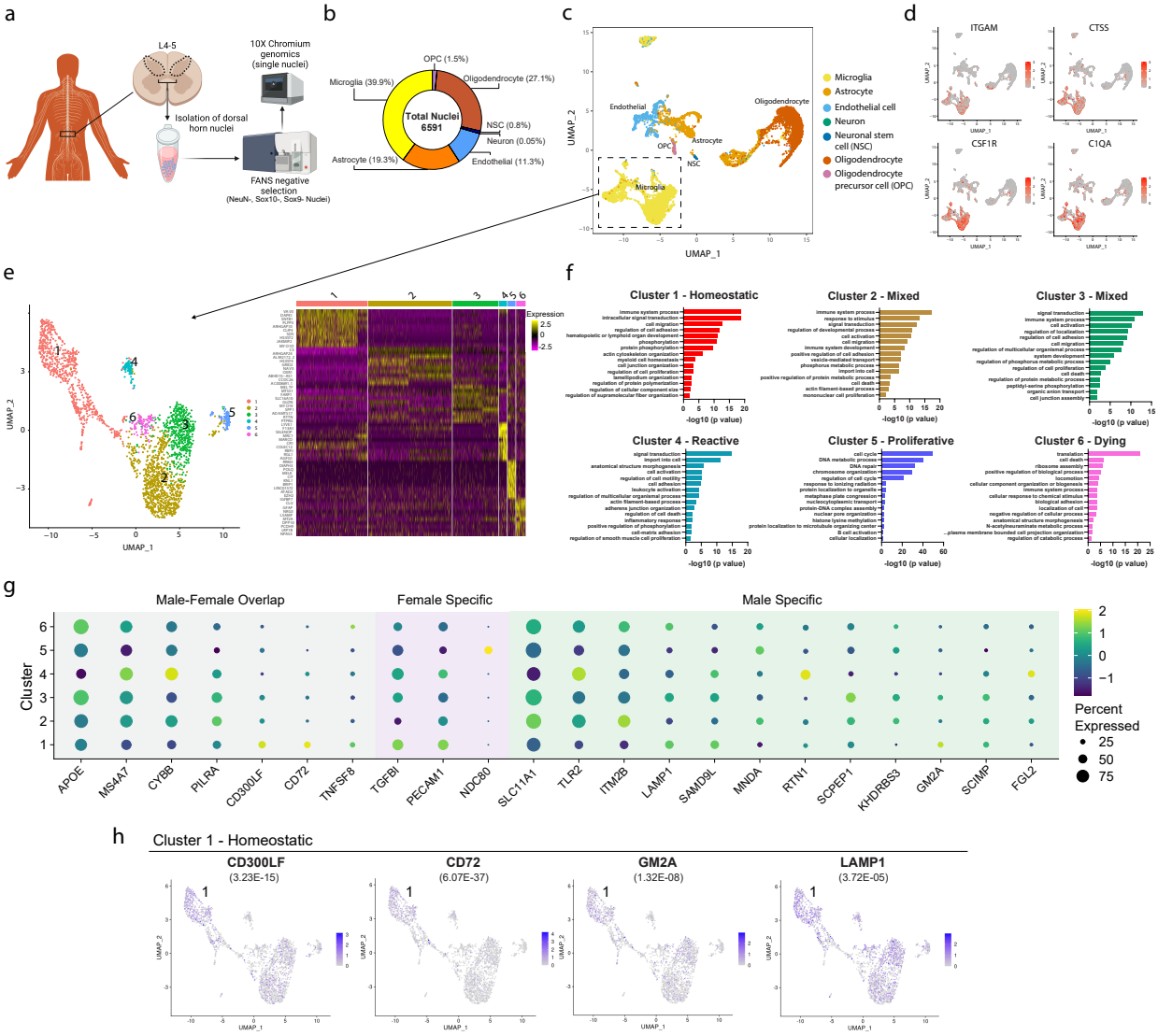

Figure 6. Single-nuclei RNA-sequencing (snRNA-seq) of human microglia uncovers gene targets identified in repopulated microglia. a) Diagram depicting experimental flow of isolation and enrichment of microglial nuclei from human dorsal horn spinal cord grey matter and subsequent 10X Chromium sequencing. b) Percentages of cell-type specific nuclei captured and sequenced, with microglia enriched to 40% of total nuclei. c) Uniform manifold approximation and projection (UMAP) projection showing distribution of human spinal cord single nuclei clusters by cell-type. Dashed box indicates final microglial clusters that were further sub-clustered in panel *e*. d) Microglial-specific cell clusters are identified using known microglia gene markers. e) Six distinct microglial nuclei clusters were identified after sub-clustering using Seurat. f) Gene ontology (GO) analysis showing top 15 GO terms that capture differential microglia cell states. g) Dot plot of selected top mouse genes that were significantly differentially expressed between human microglial subclusters (cluster 1-6). Genes that overlap in male/female mouse datasets shown in the grey zone, female-specific genes shown in the purple zone, and male-specific genes in green zone. h) UMAP plots showing genes significantly highly expressed in the human homeostatic cluster 1, also upregulated in injured-repopulated mouse microglia. p-value from

1370 differential cluster-expression analysis shown in parentheses below gene name. Scale bar
1371 represents relative gene expression.